

## On p21 Tracking Property in Cancer Cell Unravelling Bio-Digitally *in silico*. Are Apoptosis Principles Universal?

R. M. Ardito Marretta<sup>\*,†</sup> and G. Barbaraci<sup>‡</sup>

**Abstract:** Upon severe DNA damage, p21 acts in a dual mode; on the one hand, it inhibits the cyclin-CDK complex for arresting the  $G_2/M$  transition and on the other hand, it indirectly becomes an apoptotic factor by activating - in sequence - the retinoblastoma protein, E2F1 and APAF1 expressions. But, in a cancer cells proliferation, the mechanisms of, and participants in, the apoptosis failure remain unclear. Since the p21/p53/Mdm2 proteins network normally involves a digital response in a cancer cell, through an original design of a cell signalling-protein simulator, we demonstrate, *in silico*, that apoptosis phase instability is fully reciprocated by p21mRNA irregular dynamics which operates according to a "tracking memory" principle. We show p21mRNA paradoxically ceases to act in concert with specific target genes and becomes an underlying accomplice of cancer proliferation. Here, we also identify the mechanisms for allowing the cancer cell to re-enter inside a steady stable apoptosis phase.

**Keywords:** cancer cell apoptosis, digital cell biology, protein signalling, protein networks

### 1 Introduction

Nowadays, in the cancer pathologies, great attention has been paid to the oncosuppressor p53 protein and its ability to induce the transcription of genes in charge of the cell-cycle arrest, DNA repair and apoptosis [1, 2, 3, 4, 5]. For example, the well-known Knudson model of tumorigene-

sis draws the conclusion that mutation of both copies of each gene of this oncosuppressor is necessary and sufficient to trigger neoplasm formation [6, 7, 8]. But, other studies [9, 10] experimentally show how haploinsufficiency can violate Knudson's hypothesis, e.g., tumours can arise in mice with only one undamaged copy of the p53 transcription factor.

In the cell-cycle arrest and the DNA repair actions, p53 is not a "stand-alone" actor but works in synchrony with the Mdm2 protein through ubiquitin-mediated proteolysis in such a way as to realize a biological negative feedback in which the p53 level is kept low [4]. Subsequently, upon DNA damage, the ATM protein (Ataxia-Telangectasia-Mutated) kinase acts to phosphorylate the p53 to avoid binding of the Mdm2. Mainly, these degradation actions occur in the nucleus and they are confirmed and well-predicted, respectively, both from experimental procedures and mathematical kinases simulations [11, 12, 13, 14, 15, 16, 17, 18]. In a human cell, the biological response of the species considered (ATM, p53 and Mdm2) is interlinked with, and quite similar to, the output response of oscillating network dynamics, i.e., ( $ATM \rightarrow p53 \rightarrow Mdm2 \mapsto |p53$ ).

If DNA damage exceeds a threshold, the p53 pulses to activate transcription of the p21 gene and other species for apoptosis execution [19, 20, 21, 22, 23].

Even though experimental and theoretical biological studies try to clarify the mechanisms generating apoptosis triggering in a human cell when its DNA contains irreversible damage, the crux of the problem arises from an unresolved question: in this case, how does a cancer cell outflank apoptosis? In the recent past, to answer this question, attention has been focussed on the

\* Department of Structural, Aerospace Engineering and Geotechnics, University of Palermo, Viale delle Scienze, Block 8, 90128, Palermo, Italy

† Corresponding author. Tel.: +39-91-6459912; Fax: +39-91-485439; Email: romario@unipa.it

‡ Department of Mechanical Engineering, University of Palermo, Viale delle Scienze, 90128, Palermo, Italy

p53/Mdm2 network [24] and its three jobs, i.e., arrest of cell progression, prevention of DNA damage and cell death. But it has long been puzzling how p53 chooses between two options for cell fate [25, 26, 27]. The common guideline for experimentally approaching the apoptosis mechanism takes into account that mutation of the control network species for apoptosis control can modify cell fate from the wild-type response. On the other hand, it is recognized that apoptosis triggers in wild-type cells having greater DNA damage but when p21 (or Wip1) is overexpressed this doesn't occur, the threshold limit of the DNA damage being the crucial environmental parameter.

When p21 protein triggers - in cascade - inhibition of the cyclin-CDK complex occurs to assign a delay in the  $G_2/M$  cell phases (arrest) and a signalling-dialogue activates other target genes involved in cell apoptosis [5].

On the basis of our recent studies [21, 22, 23], a single-cell kinases digital virtual simulator was developed to generally predict the cell defence machinery response under cancer attack and specifically to detect the p21 protein dynamics in the apoptosis phase. Intriguingly, when DNA damage is severe, activating p21mRNA overexpression appears critical for the mechanism of the apoptotic protease activating factors (APAF1, DINP1, AIP1 and cytoc) which are triggered downstream by the signalling of the p53/Mdm2 network to decide on cell fate as extreme defence. In this new study, based on our previous results[23], we demonstrate that the apoptosis evolution, in a damaged cell, is strongly affected by p21mRNA gene dynamics. Moreover, we unravel the double-cross mechanism of its unsteady evolution which tricks the mechanism by which cell fate switches between "repair and survive" or "give up and die". We show that p21mRNA redirects cell fate by exploiting two co-factors; first, its p53-independent time-variant overexpression dynamics and secondly, an unexpected digital "tracking mode" property for pointwise targeting of the other apoptotic gene pathways within their time-rate inversions.

In all the performed cancer cell digital simulations *in silico*, this p21mRNA "tracking" property

remains a constant feature, then universal, apart from the level of the DNA damage; most probably, it acts in other human diseases different from cancer pathologies.

Once this principle is identified as universal, consequently, the proposed cell digital simulator is useful to demonstrate how the whole cell apoptosis network rigorously falls into line with this principle and to suggest the mechanism for apoptosis stimulation and stabilization.

## 2 Adopted method (Cell signalling digital design and *in silico* simulations)

The design of this virtual cell protein kinases simulator considers only the genes and proteins involved in the cellular process under examination but it could be widely generalized. All the recursive routines and digital circuitries were processed using *Matlab/Simulink* platforms at the Department of Mechanical Engineering - University of Bath (UK) - under the supervision of Doctor Michael Carley. For interested readers, this section briefly describes the design philosophy and digital tools. For human single-cell processing, we consider the p53 protein forms: p53 mono-ubiquitinated, p53 poly-ubiquitinated and p53 total ( $p53_U$ ,  $p53_{UU}$  and  $p53_{tot}$ , respectively) and Mdm2 nuclear, cytoplasmic and phosphorylated ( $Mdm2_{nuc}$ ,  $Mdm2_{cyt}$  and  $Mdm2_{P_{cyt}}$ , respectively) and their time-dependency from a mathematical model [4]. The digital translation of the p53 time rate concentration is represented by

$$\underline{x}(t) \triangleq \begin{bmatrix} [p53] [p53_U] [p53_{UU}] [p\dot{5}3] [p\dot{5}3_U] [p\dot{5}3_{UU}] \end{bmatrix}^T \quad (1)$$

where the overdot represents the time-derivative and the symbols  $U$ ,  $UU$  identify the first-, the poly-ubiquitin protein forms and  $T$  (upper the right-hand square bracket) the transpose of the vector, respectively.

According to the signalling nature of the genes involved in the present work, a digital feedback design circuit was conceived and obtained by vector

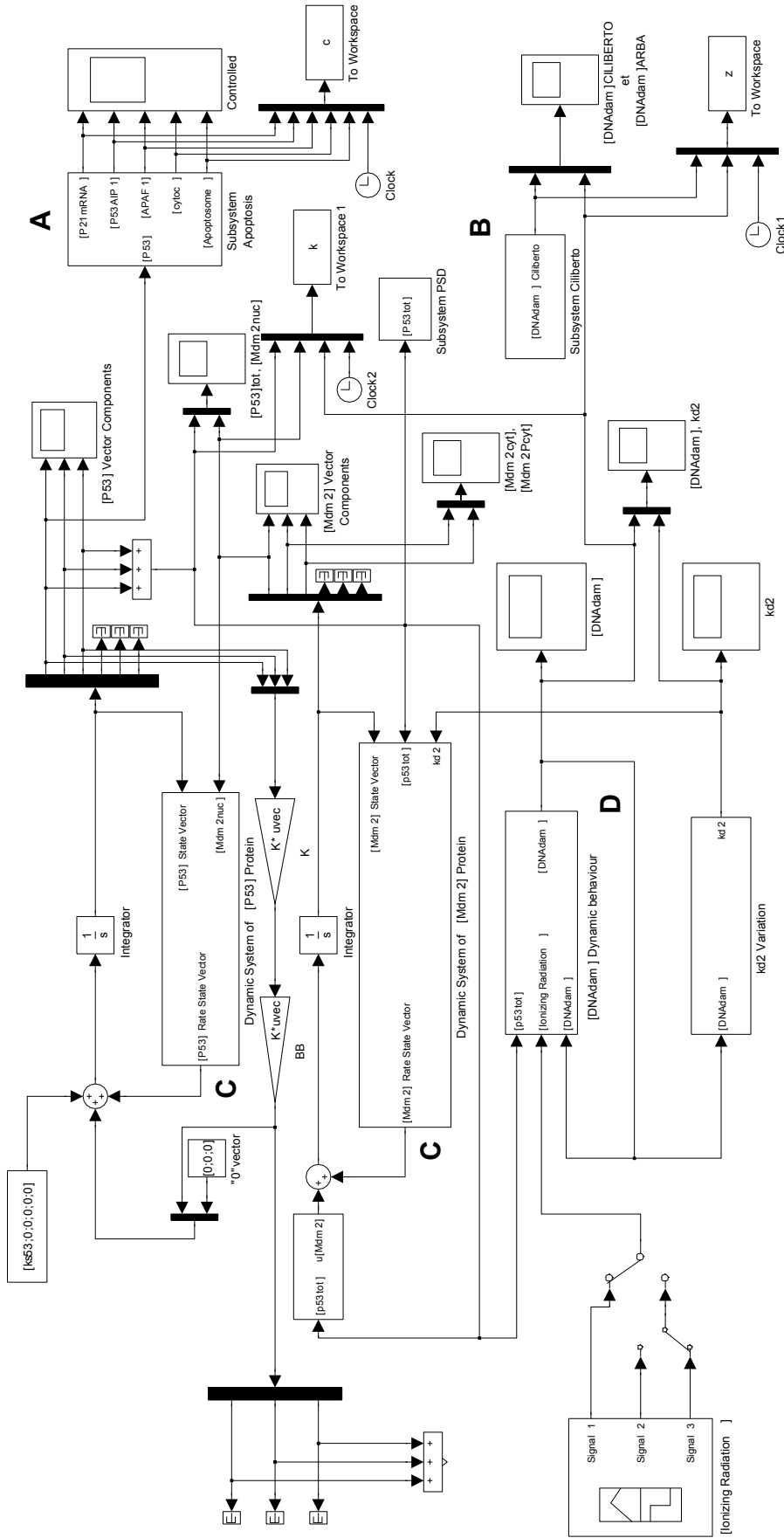


**Figure 1: Human cell master digital simulator (overall view)** - The main blocks (see close-up views) calculate the p53/Mdm2/DNA network dynamics once the input signal of ionizing radiation is processed by sub-block D; both p53/Mdm2 positive/negative feedback loops are generated and digitally processed through sub-blocks C (see close-up view). A control matrix (CPU) is located between the two sub-blocks C for a real-time check of the digital output variables (protein kinases and their time rates). The onset of sub-block B (see close-up view) is tuned to accurately replicate the results of the literature regarding irreversible and reversible DNA damage levels. Sub-block A (see close-up view) is designed to simulate the apoptotic target genes for apoptosis (p21mRNA, p53AIP1, APAF1, cytoC and Apoptosome). Oscillatory scopes are added for monitoring the involved pulsing species over the assigned time-span.

### APOPTOSIS NETWORK SUB -BLOCK A

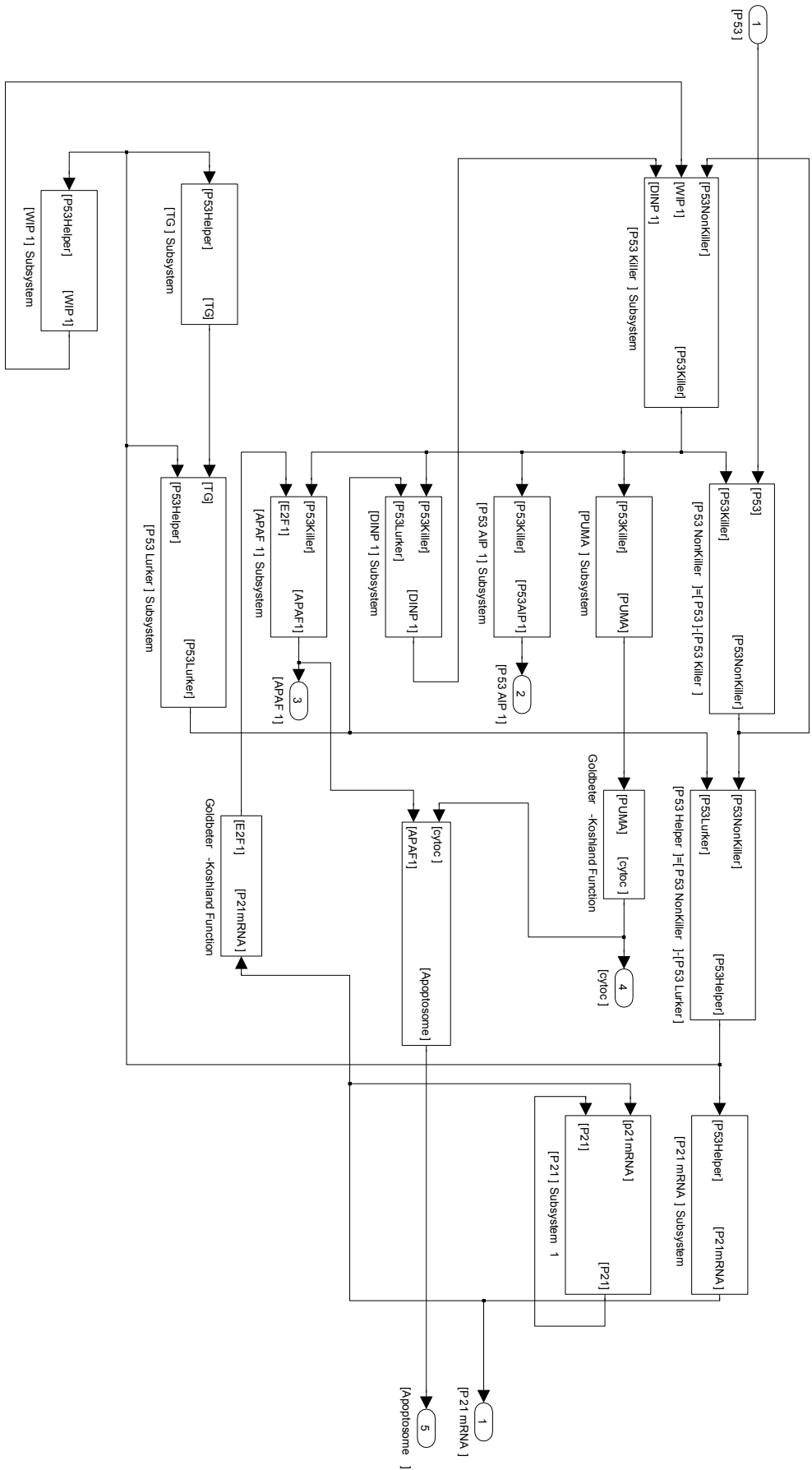
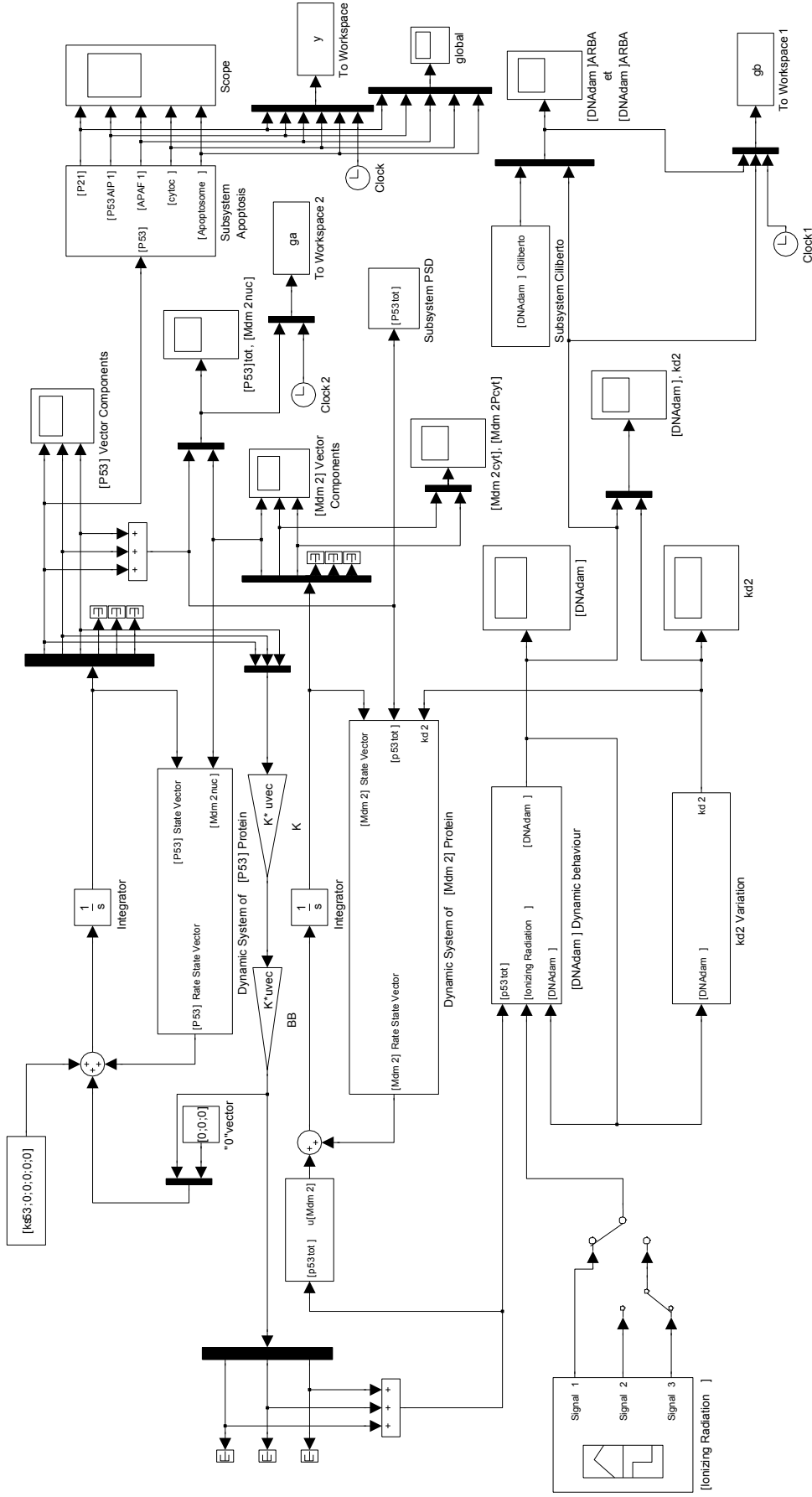
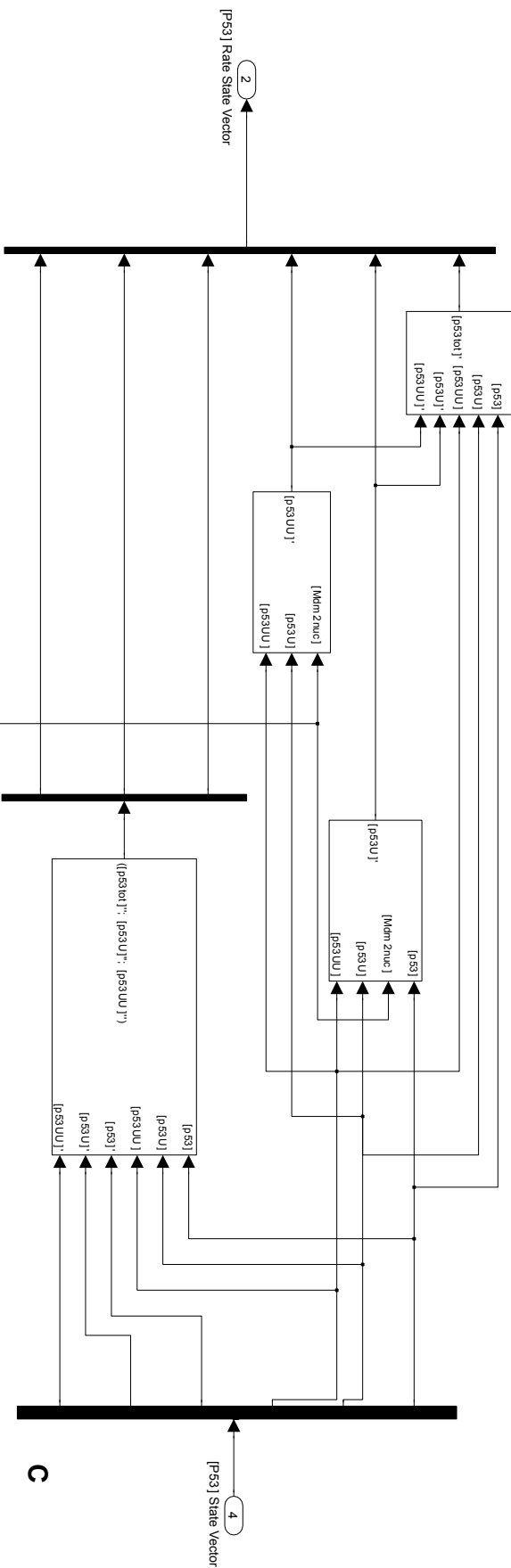


Figure 1: **Sub-block A - apoptosis network sub-block** - If *p53<sup>helper</sup>*-induced phosphatase Wip1 exceeds *p53<sup>lurker</sup>*-induced kinase p53DINP1, then *p53* signals consist of "helpers" and "lurkers". As Wip1 decreases while *p53DINP1* increases, via transformation of *p53<sup>helper</sup>* into *p53<sup>lurker</sup>*, *p53<sup>killer</sup>* begins to accumulate (Wip1 and *p53<sup>killer</sup>* subsystems). If DNA damage is quickly repaired, PUMA, *p53AIP1*, *p53DINP1* and APAF1 subsystems are not activated. On severe DNA damage the apoptosis network starts to pulse for accumulation of *p53<sup>killer</sup>* and PUMA-cytoc, *p53<sup>helper</sup>*: Apoptosome and *p21* mRNA subsystems are designed to match a steady-stable apoptosis phase.

### SUB-BLOCK B



**Figure 1: Sub-block B. - p53/Mdm2/DNA damage network sub-block** - Negative/positive digital p53/Mdm2/DNA damage feedback loops run inside the central core of the block-diagram ( $p53_{tot}$ ,  $Mdm2$ ,  $k_{d2}$  subsystems). The kinases digital protocols require that nuclear form of Mdm2 bind two ubiquitins to p53, first converting p53 into a monoubiquitinated form and then converting it into polyubiquitinated p53. The cell virtual master simulator considers that four molecules of p53 form a tetramer. Inside the blocks Mdm2 is phosphorylated by ATK protein. The final step obtains the conversion of cytoplasmic Mdm2 into phosphorylated  $Mdm2_{P_{Cyt}}$ . Then, the positive feedback loop is digitally realized by the reaction scheme:  $p53 \rightarrow PTEN \rightarrow PIP3 \rightarrow AKT \rightarrow Mdm2_{nuc} \rightarrow p53$  (in which PTEN and PIP3 are protein phosphatase and Phosphatidylinositol-tris-phosphate, respectively).



**DIGITAL FEEDBACK p53/Mdm2/DNA damage NETWORK SUB-BLOCKS C, D**

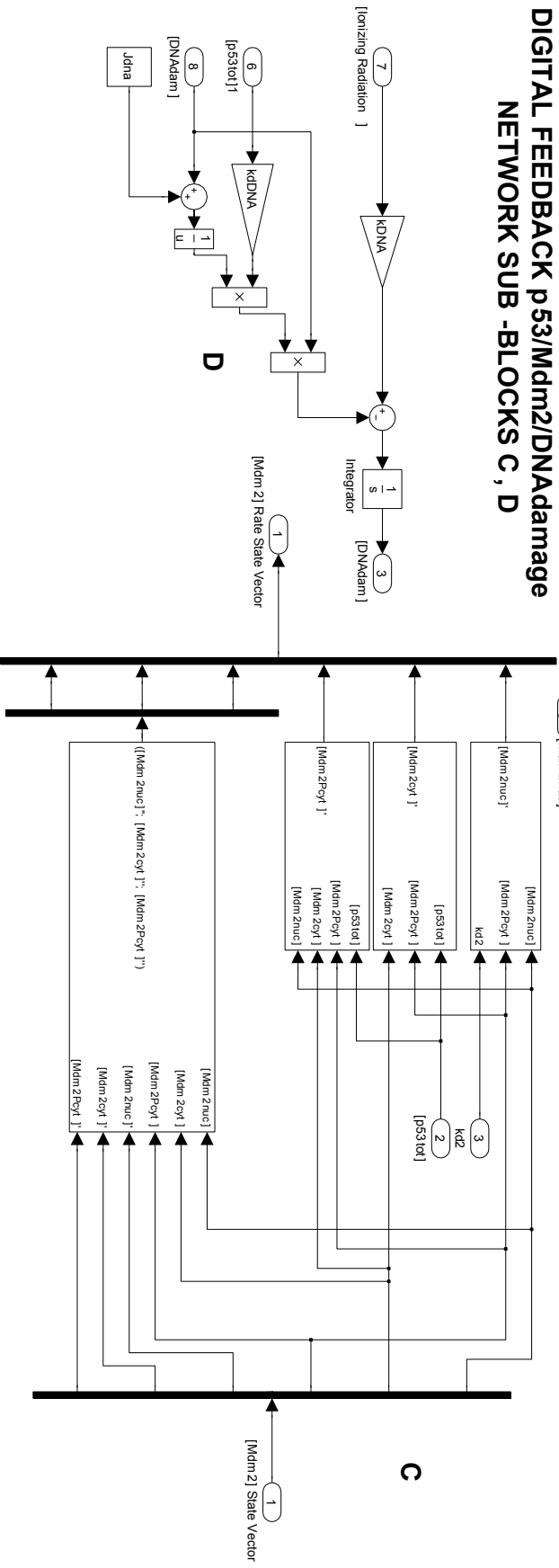


Figure 1: **Sub-blocks C-D. - p53/Mdm2/DNA damage network sub-blocks** - Protein kinases circuitry digitally converts the two feedback loops between p53 and Mdm2 (sub-blocks C). The interlinked sub-block D has two digital tasks: 1) it gives as input the ionizing signal for assigning a DNA damage threshold, and, 2) it receives the output response of the p53/Mdm2 repairing action.

expressions:

$$d\mathbf{x}/dt = f(Mdm2_{nuc}(t), \mathbf{x}(t), \mathbf{b}) \quad (2)$$

$$\underline{z}(t) \triangleq [[Mdm2_{nuc}] [Mdm2_{cyt}] [Mdm2_{p_{cyt}}] [Mdm2_{nuc}] [Mdm2_{cyt}] [Mdm2_{p_{cyt}}]]^T \quad (3)$$

$$d\mathbf{z}/dt = f(k_{d2}, p53_{tot}(t), \mathbf{z}(t), \mathbf{c}) \quad (4)$$

$$\underline{c}(t) \triangleq [0 f([p53_{tot}(t)]) 0000]^T \quad (5)$$

where  $Mdm2_{nuc}(t)$  defines the time-dependent oncogene concentration rate in nuclear form during the DNA repairing action; while,  $Mdm2_{cyt}(t)$  and  $Mdm2_{p_{cyt}}(t)$  are the time-dependent oncogene concentration rates in cytoplasmic and phosphorylated forms, respectively;  $k_{d2}(t)$  is the rate constant for degradation of  $Mdm2_{nuc}(t)$ ; meanwhile, all the blacked quantities above mentioned are denoting time varying scalar quantities. In Eqs. (2), (4) and (5), the functional form of the function  $f$  is different for each relation being  $f$  dependent (in chain) from the genes concentration rate, the state-vectors  $\mathbf{x}(t)$  and  $\mathbf{z}(t)$ , the rate constant of degradation  $k_{d2}(t)$  and the transition input-state vectors of p53 and Mdm2 dynamics  $\mathbf{b}$  and  $\mathbf{c}$ , respectively. Thus, the employed (and common) functional  $f$  becomes a typical and generic mathematical symbol. Also, the function  $f$  employed both in the Eqs. (2) and (4) is representative of a linear transformation typical of state-space dynamics.

The digital circuitry also models the interlinked networks of the apoptotic species, p21mRNA ( $m_{21}$ ) and the time rate of DNA damage ( $DNA_{dam}$ ) by the following system of equations:

$$\frac{dm_{21}}{dt} = \gamma_m m_{21} - j_{21} \frac{k_a''}{k_a'' + k_d''} \quad (6)$$

$$\frac{dp_{21}}{dt} = j_{p21} m_{21} - \gamma_{p21} p_{21} \quad (7)$$

$$\frac{d[DNA_{dam}]}{dt} = kDNA[IR] - k_d DNA [p53_{tot}] \frac{[DNA_{dam}]}{J_{DNA} + [DNA_{dam}]} \quad (8)$$

in which  $IR$  represents the functional of the imposed radiation dose and  $\gamma_m, p_{21}, j_{21}, j_{p21}$  and  $k_{a,d}''$  are the time rate kinases coefficients interlinked to the apoptotic network including the p53AIP1, APAF1, cytoc and Apoptosome target genes. It is worth to note the quantities  $\gamma_m, m_{21}, p_{21}, j_{21}, j_{p21}, \gamma_{p21}$  and the other quantities in Eqs. (6), (7) and (8) are defined according to the time rate kinase coefficients regarding the apoptotic target species p53AIP1, APAF1, cytochrome and caspase 8 dynamics. They are representative of the time rate constants of the involved species kinases.

### 3 Results and discussions

#### 3.1 Activated p21 prevents excess DNA damage accumulation but aberrant super-activation pathways of p21mRNA can become super-critical - simulator response *in silico* concerning p21mRNA in presence of DNA damage

Since the p21/p53/Mdm2 and apoptosis target gene networks are interlinked via digital signalling dynamics, the present authors designed *ex novo* a virtual kinases master control simulator (Figures 1-4) capable of reproducing and predicting the mutual pulsing actions of the involved species. In that previous work[23], the cell digital simulator was tuned for matching the experimentally observed oscillations of the p53/Mdm2 proteins network. Indeed, in that same study[23], digital simulations give preliminary remarks about p21 influence on the apoptotic genes network once it has been expressed with Wip1 and earlier than the apoptotic species, p53DINP1 and p53AIP1 [28, 29]. However, this result was in agreement to outstanding recent work[30] regarding the suspicious behaviour of p21 and its activities.

In fact, it is actually conceived that, for a damaged cell, p53 accumulates and modifies the in-

tracellular context through gene induction, allowing the cell control system to store a "memory" of the damage. As shown in Figures 5 and 7, the obtained results fit well those in literature.

Conversely, even though the p53/Mdm2 stand-alone model is a good biological reference frame for describing agents and processes of cell cycles, we think it remains too speculative for two reasons: firstly, because it involves, as a consequence, that apoptotic response depends on the dose and inter-dose interval of the DNA-damaging irradiation, and, secondly, it is unable to find the inner mechanism linking the overexpression of p21 and Wip1 to the apoptosis execution.

In the present study, we start to change that biological perspective and some methodological approaches, taken as frames of mind, like those of Tsourkas and Weissleder[31], Deguchi, Ohashi and Sato[32], Mooney[33], Zhou, Chen and Zhang [34] seem useful for the present goal.

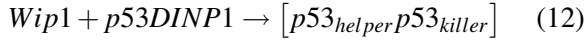
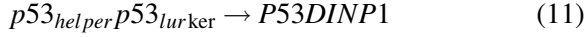
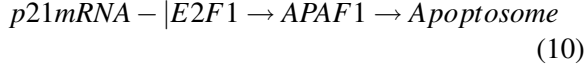
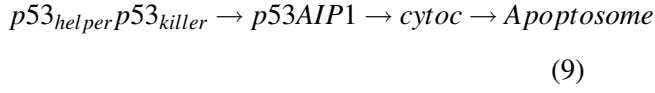
The first run of our digital test bank is performed to show consistency with experimental data in terms of proteins responses both to reversible and irreversible DNA damages (Figures 5-7). Initial simulator shakedown takes into account the reference genes investigated earlier (in both responses) i.e., the total p53 ( $p53_{tot}$ ) and the nuclear Mdm2 ( $Mdm2_{nuc}$ ) for paving the way to the next step to come.

In this context, we simulate a human cell both reversibly and irreversibly damaged and observe (Figure 6) how the (over)expression of p21 is quiescent at the beginning of the apoptotic time-window. Its overexpression triggering comes almost suddenly with a concurrent closure of the apoptotic time-window so as to allow the cell to avoid its fate.

As previously mentioned, a master control digital cell simulator (Figures 1-4) - *ad hoc* conceived - successfully matches the experimental results of interest in pre-processing p53/Mdm2 and wild-type networks when DNA damage is present. Its design engineering concepts are probably not familiar to a biology audience and, here, they do not become matter of study. Very con-

cisely, it was implemented as a digital system able to reproduce both the species kinases and the digital signalling of the p53/Mdm2/p21mRNA and wild-types APAF1/p53AIP1/CytoC networks [4, 5, 19, 20]. This biological multi-tasking simulator is totally generalized and potentially applicable to other wild-type-dependent species (the interested readers can find the outcome reproducibility in a devoted section of this paper regarding the methods set-up). The reliability of the present digital method is even more marked when opposite conditions are under examination, i.e., a quickly repaired and an irreversible DNA damage level, respectively. In the first case,  $p53_{tot}$  (total amount of p53) and  $Mdm2_{nuc}$  (nuclear form of the oncogene) are involved in both a positive and a negative back-reaction in which  $Mdm2_{nuc}$  induces p53 degradation while p53 inhibits nuclear entry of Mdm2 according to the scheme:  $p53_{tot} \rightarrow Mdm2_{cyt} \rightarrow Mdm2_{nuc} \mapsto |p53_{tot}$  (where  $Mdm2_{cyt}$  represents the cytoplasmic form). The final cell net gain is concisely resumed in the drop in  $p53_{tot}$  which cuts off the synthesis of cytoplasmic Mdm2;  $p53_{tot}$  starts to rise again due to the low level of  $Mdm2_{nuc}$  and a new oscillation starts (Figure 5). The cell digital circuitry behaves consistently and we faithfully reproduce the network experimental oscillations, the onset of the cell master virtual simulator being tuned on the optimal repairing speed of DNA damage. A very slight discrepancy between experimentally and digitally  $p53_{tot}$  levels has not effect on this new approach. On the other hand, even though low level DNA damage is present (and only two ends of phosphorylation of p53 are considered in the first instance), in spite of the activation of the repair network, we model the concurrent cell defence machinery which activates a check-point procedure for maintaining apoptosis in stand-by configuration. In this model, while the cytochrome C is released (Apoptosome), it binds to the cytosolic protein APAF1 and the Caspase8-dependent cytoc is activated (Figure 6); the wild-type of p53 (p53AIP1) is tetra-dependent both on E2F1 (inhibited by p21) and on three forms of p53 wild-type ( $p53_{killer}$ ,  $p53_{lurker}$  and  $p53_{helper}$ ). The resulting kinases scheme - experimentally confirmed and digitally translated - displays the path-

ways of species in Figure 6.



The third kinase being in back-reaction.

For the sake of simplicity, we used Eqs. (9)-(11) as pathways in compact form. Massive details of the quantitative relations can be found in Ref. [5]. Here, for reader convenience, they are resumed:

$$\frac{d[p53_{killer}]}{dt} = [DINP1] \cdot \frac{[p53_{nonkiller}]}{0.1 + [p53_{nonkiller}]} - [Wip1] \cdot \frac{[p53_{killer}]}{0.1 + [p53_{killer}]}$$

$$\frac{d[p53_{turker}]}{dt} = k_{TGp53} \cdot [TG] \frac{[p53_{helper}]}{0.1 + [p53_{helper}]} - \theta_{TG} \cdot \frac{[p53_{turker}]}{0.1 + [p53_{turker}]}$$

$$[p53_{helper}] = [p53_{nonkiller}] - [p53_{turker}]$$

$$\frac{d[p53AIP1]}{dt} = k'_{sp53AIP1} + k''_{sp53AIP1} \cdot \frac{[p53_{killer}]^3}{J_{sp53AIP1}^3 + [p53_{killer}]^3} - k_{dp53AIP1}[p53AIP1]$$

$$\frac{d[APAF1]}{dt} = k'_{sAPAF1} + k''_{sAPAF1} \cdot \frac{[p53_{killer}]^3}{J_{sp53killer}^3 + [p53_{killer}]^3} \cdot \frac{[E2F1]^3}{J_{E2F1}^3 + [E2F1]^3} - k_{dAPAF1}[APAF1]$$

$$[\text{cytoc}] = G([PUMA], \theta_{PUMA}, 0.1, 0.1)$$

$$[\text{Apoptosome}] = H([APAF1] - \theta_{APAF1}) * H([\text{cytoc}] - \theta_{cytoc})$$

Where G and H are the Goldbeter-Koshland and Heaviside functions, respectively. We now compare conceptually the results displayed in Figure 6 with those of the most recent literature. In an outstanding experimental work [30], analysis of the effects of PML-RAR on p21 in p53 for leukaemia

stem cells showed that, indeed, p21 upregulation by PML-RAR is p53 independent. By superimposing Figure 5 upon Figure 6, the proposed network signaling (for two pulses) shows a frequency of  $7.4 \times 10^{-5}$  vs.  $7.092 \times 10^{-5}$  [30] and a relative error of 4 %. But these digital data bear important implication for confirming the p53-independent p21 upregulation and resolving the uncertainty about the consequences of induced DNA damage. We think timescales and time-rates of the gene dynamics can crack the cell biological code for the present goal. From the above mentioned figures, one has to note the clock frequency is directly tuned by p53/Mdm2 signals corresponding to the unsteady amount of DNA damage. The delay (and phase-shift) in the response of  $p53_{tot}$  are evident when the highest level of DNA damage is present. This is due to the natural "inertia" of the cell defense machinery in activating pulses of its transcription factors (the DNA repair frequency being shifted by  $3.3 \times 10^{-4}$ ). The amplitudes and modal frequencies of the proteins involved are totally dependent on the local DNA damage gradient (see Figure 5) or its pathway slopes (a faster repair action belongs to the interval  $0 \div 250$ min, while the interval  $250 \div 600$ min shows a lower speed DNA repair). If one now takes into account the p21mRNA network dynamics (Figure 6) in the time-window  $100 \div \approx 200$ min, a double-crossing game can be bio-digittally unravelled. In agreement with to but differently from Viale and colleagues [30], we deduce that p21 upregulation is p53-independent but this is true along the initial frame of time-span ( $0 \div \approx 200$ min). The discrepancy between our results and those of these authors is superficial. In fact, the overexpression of p21 digittally triggers in a very small interval and its intensity (and gradient), more similar to a Dirac impulse, is quite different to those of the other gene expressions. This behavior, typically digital, implies two effects: first, p21mRNA upregulation becomes almost "invisible" when one has to evaluate its effects in back-reactions and experimental tools might fail to find it unless they have a suitable digital interface setup; secondly, if one admits as negligible the p53-dependence of p21mRNA overexpression, this could become supercritical for the apoptotic network.

### 3.2 p21 response dynamics runs like a "tracking signalling radome" for targeting the apoptotic network gene time-rate inversions

During a repair action of the DNA damage, two devoted cell networks are accomplishing their tasks. While the first checks the amount of damage and starts to pulse its components (p53/Mdm2) via ATM pathways and cyclin CDK complex activation, the second is ready in stand-by configuration. According to the proposed bio-digital model, for an overall timescale of 1200min, p21mRNA upregulation is p53-independent for about 120min, while the other considered species and p53 wild-types show low-intensity gradients (Figure 6) with positive slow growth factors. The apoptotic network switches on the alert at an exact time location, i.e., when the target gene gradients - even though growing up - start to invert their time rates. This convergence criterion leads the gene gradients for decrypting the apoptosis code. When this occurs, the apoptotic target genes coherently trigger to match the cell death, while the p53/Mdm2 network goes on by a signaling-dialogue for giving/receiving information to/from p21mRNA-based network. If the speed of repair action is very high (see Figure 5 over the first 120min), p21 immediately triggers to its highest time rate. The other target species gradients (time rates) almost vanish (only wild-type APAF1 shows inversion of its time rate) and the apoptosis is then switched off. We investigated the p21mRNA expression and cell cycle to find if the first is critical in maintaining the cell cycle in apoptosis regime when a threshold limit of DNA damage is overcome. In other words, we try to find if the p21mRNA gene is capable of betraying the signalling-dialogue with the p53/Mdm2 network, and, worse still, if (and when) p21mRNA acts downstream with malignant latency to lead to damaged cell proliferation. In this work, we reproduce, *in silico*, the signaling digital nature of the considered gene network and we observe that p21mRNA maintains its overexpression in such a way as to be p53 pulse-independent. Then, to analyze the subject clearly and relate it to the generation of p21-dependent

target genes inter-dynamics, we consider a cell having a DNA damage level beyond the threshold limit. In our master digital cell species simulator this is easy to achieve by commuting the input signal level of the DNA damage to the target gene network block into a constant value. As a consequence, and consistently, the response of the p53/Mdm2 network radically changes. The  $p53_{tot}$  output signal is now changed into an impulse train of prolonged undamped oscillations (Figure 7) whose amplitude and frequency - now one order higher ( $1.15 \times 10^{-4}$ ) than the first case in which the DNA was quickly repaired - are in agreement with those of literature [19, 20].

Having successfully checked the reliability of the employed cell network simulator, we show how p21mRNA signaling plays a prominent role in apoptosis, paradoxically switching from cell-cycle tester gene to promoter of potential cancer propagation. When irreversible DNA damage is present, the p53/Mdm2 network undergoes prolonged and undamped pulses while the apoptotic species network shows something different (Figure 8). Once again, all the target genes range themselves in such a way that their inflection points (time rate inversions) occur with the same sense and - as expected - apoptosis phase triggers as shown in Figure 9 (apoptosis is matched or not if the Apoptosome target gene digital index is equal to 1 or 0, respectively). Instead, p21mRNA again shows its overexpression but with a different pathway from the previous case (in which the DNA damage was quickly repaired). It seems p21mRNA acts like a "radio-frequency tracking radome" to instantly identify the wavelengths and frequencies of the apoptotic species and intercept their gradient inversions. When this successfully occurs, it gives, in combination, the highest time rate overexpression just in phase with the lowest regulation of the other target genes. The apoptosis phase stops and the signaling-dialogue to/from p53/Mdm2 is now irrelevant. Since the interlinked [p53/Mdm2/DNA damage] and [p21mRNA/p53AIP1/APAF1/cytoc/Apoptosome] networks come into play in a digital field, we adopt a digital technique for two goals: 1) the investigation of the latter network response for

different p21mRNA pathways so as to identify a common and universal inner mechanism that leads the cancer cell to avoid apoptosis triggering, and, 2) the prediction of p21mRNA time-dependent signalling and its regulation for forcing the cancer cell to re-enter the apoptotic time-span. All the evidence of experiment and of theory is that the apoptotic target genes, induced by irreversible DNA damage, start to oscillate. In our digital model, their pulses are strongly influenced by the p21mRNA upregulation and they are not able to keep the cell death stable. A more accurate examination of the p21mRNA signal inside the apoptotic time-span, from 114.4min to 144.85min (Figures 8-10) leads to the conclusion that this protein digitally triggers in a dual mode: over a very short time span it starts like a Dirac signal and becomes a saturation signal for the remaining time-span. We take as a time reference frame the previously calculated "natural" time-span of the partial apoptosis of a cancer cell with irreversible DNA damage. To evaluate the apoptosis signal-dependency and to demonstrate the tracking property of p21mRNA, we now suppose the p21mRNA has different signal pathways over different triggering time-spans. We perform these different p21mRNA signal pathways simulations: firstly, the outfit of p21mRNA is a mono-cycle square-wave signal enclosed in three different time-spans of [0÷200min], [114.4÷144.85min (apoptotic time-window)] and [200÷1200min], respectively; afterwards, we change the mono-cycle square-wave into a negative linear-ramp signal for the p21mRNA time rate acting in the last two assigned time-spans. In the first time-span of 0÷200min, the unforeseen processed results give information about three items of interest (in this first case, p21mRNA upregulation being confined within this time-span), i.e., 1) APAF1 shows a double pulse with phase-quadrature against p21mRNA frequency ( $2.42 \times 10^{-4}$ ); 2) p21mRNA upregulation does not affect the apoptosis phase, leaving its natural frequency unchanged; 3) after the second pulse, the realized biological switch keeps the apoptosis phase active and the cell fate is fixed (Figure 11). The universal rule of the target gene gradients

(time-rates) remains confirmed when we sketch all the other species involved along the same time-span (Figures 12, 13). p21 upregulation triggers with a delay and it is not able to intersect the inflexion points of the other target genes. The conspiracy of p21mRNA is unveiled taking into account APAF1 as a marker: now, APAF1 is free to trigger its second pulse just at the end of the input signal of p21mRNA. Maliciously, p21mRNA realizes it is not able to intersect the APAF1 inflexion point time-rate and calls upon its tracking radome properties. Thus, it tries to repeat the action on the next occasion (second pulse of APAF1) but the available time-window is suddenly closed and p21mRNA burns its final chance. In corroboration of our claim, the apoptotic time-span and cycle frequency remain almost the same, i.e.,  $115.65 \div 148.1$ min and  $2.42 \times 10^{-4}$ (Figure 12). The simulations carried out for the same p21mRNA pathway (mono-cycle square-wave signal) along the other time-spans (114.4÷144.85min (apoptotic time-window) and 200÷1200min, respectively) again confirm the above assertions. The only difference is that the p21mRNA upregulation tries to intersect the APAF1 inflexion point during its first pulse (having extremely high frequency equal to  $3.61 \times 10^{-4}$ ) but the available remaining time-window is too close for a second attempt (data not shown). The apoptosis phases for both the considered time-spans remain active with unchanged double-cycle pathways and natural frequencies (data not shown). The performed simulations are useful to assess and demonstrate the potential "tracking memory" of the p21mRNA upregulation expression, but we have to check if this is a necessary and sufficient condition to obtain stable-steady apoptosis phase. As previously pointed out, we assume p21mRNA can now be represented by a negative linear-ramp signal in order to demonstrate the general rule of species time rates inversion (or their gradients signs) when apoptotic phase is requested for an irreparable cancer cell. We carry on simulations for only two time-spans (114.4÷144.85min, in phase with the apoptotic time-window, and 200÷1200min, respectively). For the first time-span, the results sketched in Figures 14-16 are

impressive. p21 upregulation almost vanishes and the remaining apoptotic species release their brakes and freely pulse toward a choral tuning at the same inflexion point at the same time location. The following apoptosis phase has no need of a second pulse and it remains permanently active. The tracking memory properties of p21mRNA are confirmed even though it is again conceived as a negative linear-ramp signal all over a time-span of 200÷1200min (i.e., past the natural apoptotic phase in the presence of irreparable DNA damage). In fact, p21mRNA upregulation immediately occurs to intersect the inflexion point of APAF1 time rate. This successfully occurs but two parameters come into play and become fatal for p21mRNA (Figures 17-19): inversion of the p21mRNA upregulation time rate and the second pulse of APAF1. p21mRNA, exploiting to the utmost its direct tracking memory access, tries to follow this second pulse of APAF1 at its inflexion point for intersection. This is allowed for the second time but the third chance is denied because APAF1 reaches a steady-stable condition. According to this pulsating species dynamics, the apoptosis phase again shows two pulses (Figure 18) and remains unchanged but with a frequency slightly lower ( $1.74 \times 10^{-4}$ ) than the natural frequency of the (unstable) apoptotic phase of a cancer cell with irreparable DNA damage.

### 3.3 p21mRNA-dependent cell control network and concurrent implications

The relevance of the problem to p21mRNA upregulation influence on apoptotic target genes network may be questioned on the grounds that it was hitherto unknown how the p21mRNA instantaneous time rate amount in a cancer cell affects cell mechanism switching properties to activate apoptosis and/or downstream target species. In light of the involved digital and extremely unsteady complex dynamics of the considered p21mRNA-network, we think its interlinked dynamic processes could be roughly estimated in laboratory. Specifically, we suggest integrating experimental biological procedures and computational tools when laboratory experiments show almost con-

flicting results or their outcome cannot be reproduced. Here, the obtained re-designed cell digital master platform machinery has been used to enhance, and build confidence in, inner mechanisms and variables of apoptosis. In the proposed method of attack, details of the p21 expressions are estimated, from biological principles and not only from the dynamics of the p21mRNA species; at the same time, as soon as the apoptotic effects are deduced, we preclude the discussion of this phenomenon where there is a significant back-reaction of the p21mRNA itself.

In all the performed simulations, the apoptotic target gene network describes a digital pathway. In a cell having irreversible DNA damage, these network digital signalling pathways seem to be of no use in steadily maintaining apoptosis triggering. Intriguingly, the digital process of the p21mRNA unravels its property to follow a "tracking memory" criterion for influencing and arresting the other target species signalling and apoptotic phases, respectively. The apoptotic phase is demonstrated to be a by-product of time rate collimation among the involved target genes, as distinct from p21mRNA upregulations. If the principle of p21mRNA tracking memory is impaired or violated, apoptotic phase shows a second pulse and it enters a permanent state. The adopted method digitally confirms that normal expression of p21 to high levels is not dependent on p53 and that induction of p21 by DNA-damaging agents does require p53. We also submit to a biological research audience the proposal that a cellular system of target genes should be devised to experimentally confirm, extend and apply the proposed model for similar or different human cell diseases. It could shed light on investigation into the mechanisms underlying stabilization methods in which the presence of proteins in cytoplasmic lysates of human RKO colorectal carcinoma cells form complexes with p21mRNA that are actually inducible by treatment with short-wavelength or other stress agents or to characterize endogenous p21 expression and transcriptional and translational inducibility of p21 in a panel of leukaemic cell lines. For example, one of the primary spin-offs of the proposed applica-

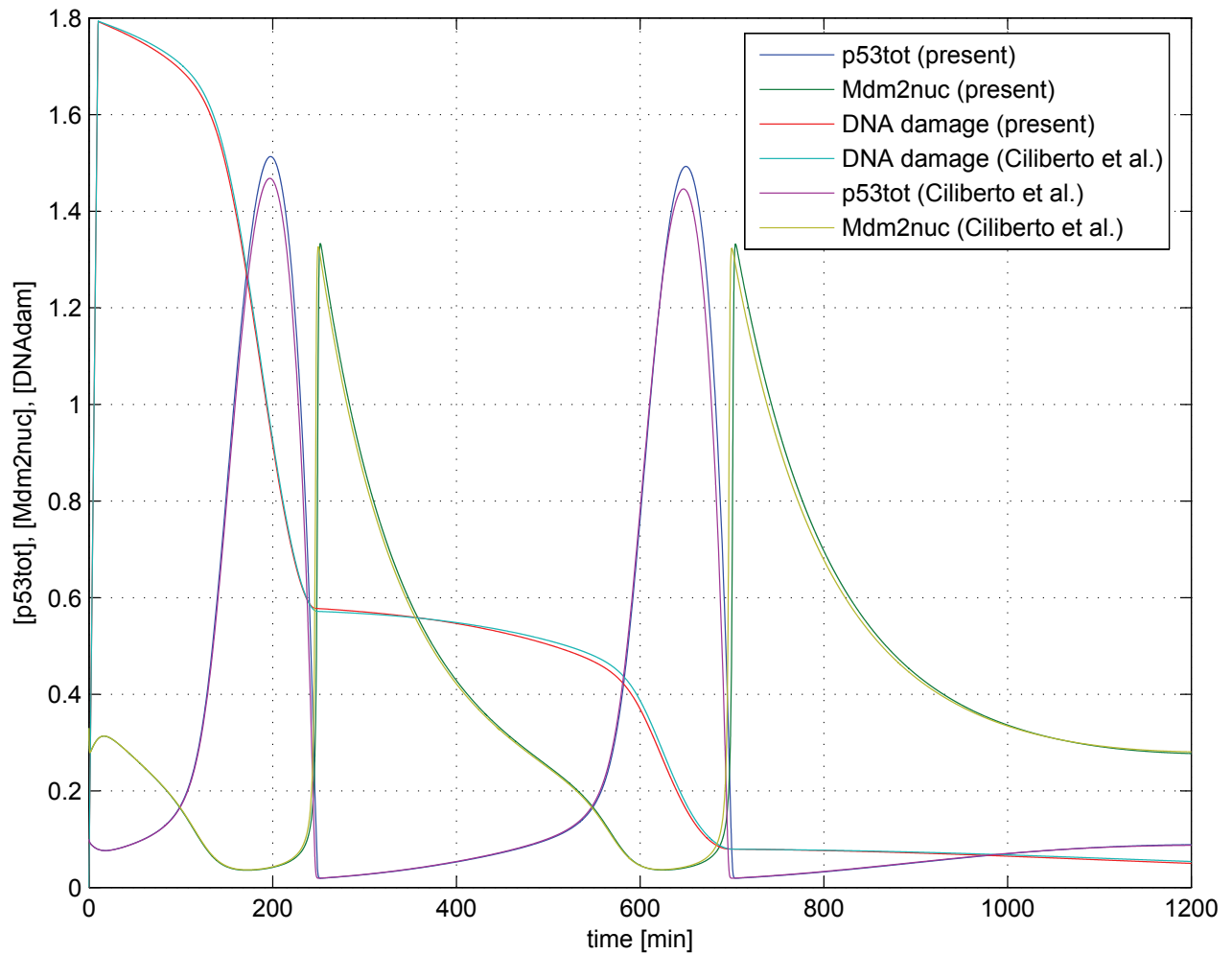


Figure 2: **Cell digital master simulator output for p53/Mdm2 vs. DNA damage repairing speed** - Output response of digital p53/Mdm2 network to gamma-irradiation dose is displayed. At the beginning of simulation, the network is at steady-state. The two pulses of  $p53_{tot}$  and  $Mdm2_{nuc}$  trigger as a consequence of  $k_{d2}$  increase which is induced by ionizing radiation,  $IR$ . When the DNA damage time-rate decreases,  $k_{d2}$  returns to its basal value. The number of pulses depends on the DNA damage threshold and the irradiation time-span and dose. A very small discrepancy between the present results and those in the literature is present only for  $p53_{tot}$ ; this is due to the onset of the digital controller which optimizes the best repair action speed through suitable wave-amplitudes of  $p53_{tot}$ .

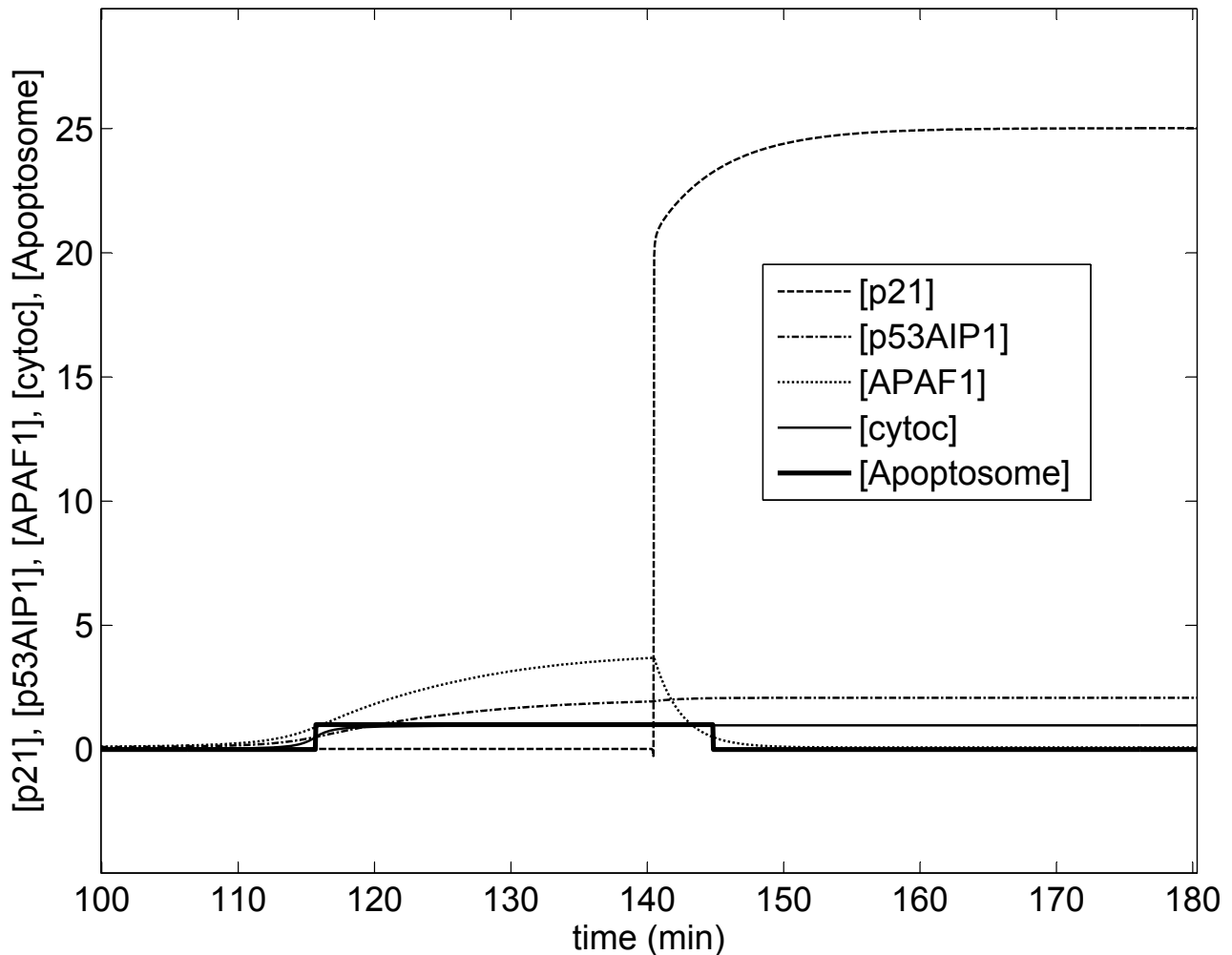


Figure 3: **Output response of apoptotic species network as a consequence of a DNA damage quickly repaired** - p21 (and Wip1, not displayed) are expressed earlier than p53DINP1 and p53AIP1 according to the experimentally observed facts (see Fiscella et al, 1997 and Oda et al, 2000). Apoptosome triggers to a digital value equal to 1 when apoptosis phase starts. This occurs when the other target genes invert their time rates all at once, p21 being almost quiescent over the complete apoptotic time-span. p21 overexpression triggers at the lowest time rates of the target genes. Specifically, p53APAF1 is induced by E2F1 (degraded by p21) and  $p53_{killer}$ ; p53AIP1 is activated by p53DINP1 via  $p53_{killer}$  and  $p53_{lurker}$ ; cytoc gene depends on PUMA via the  $p53_{lurker}$ - $p53_{helper}$  back reaction.

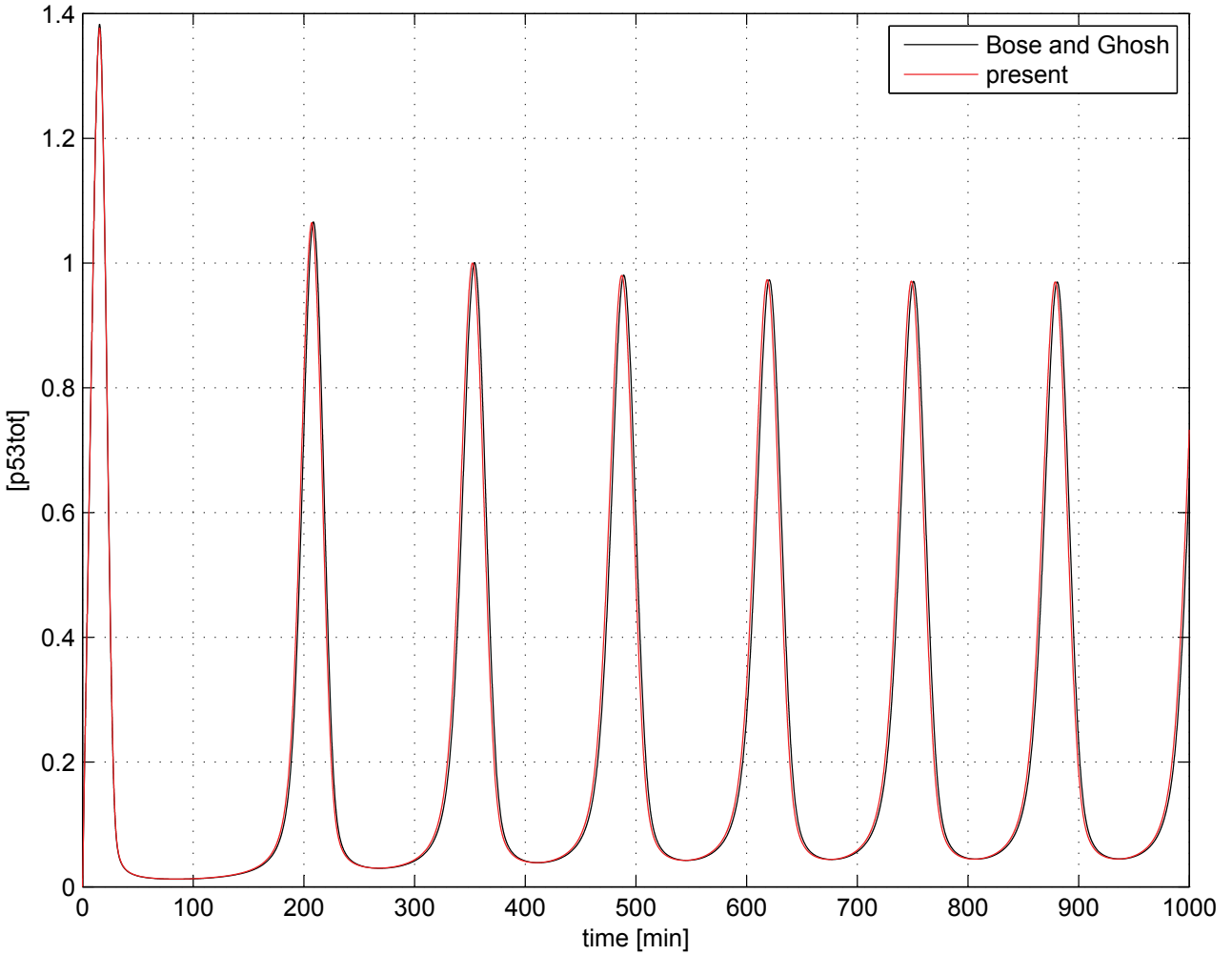


Figure 4: **Output response of  $p53_{tot}$  as a consequence of an irreversible DNA damage** - Both the inactive and active forms of p53 (tetramer) induce Mdm2 oncogene. We consider Mdm2 active state and mRNA production at rate constant. The results are consistent with experimental facts (see Lahav et al, 2004, Bose and Ghosh, 2006-2007). If  $G$  ( $G^*$ ) and  $S$  represent the inactive (active) gene and p53 tetramer, respectively, the applied reaction scheme is:  $G+S(k_m) \rightleftharpoons G-SK(k_a, k_d) \rightleftharpoons G^*(j_m) \rightarrow m_r(\gamma_m)$ . Where  $k_m$  is the equilibrium constant,  $k_a$  and  $k_d$  are the activation-deactivation rate constants,  $m_r$  the Mdm2 mRNA concentration and  $\gamma_m$  the rate constant for mRNA.

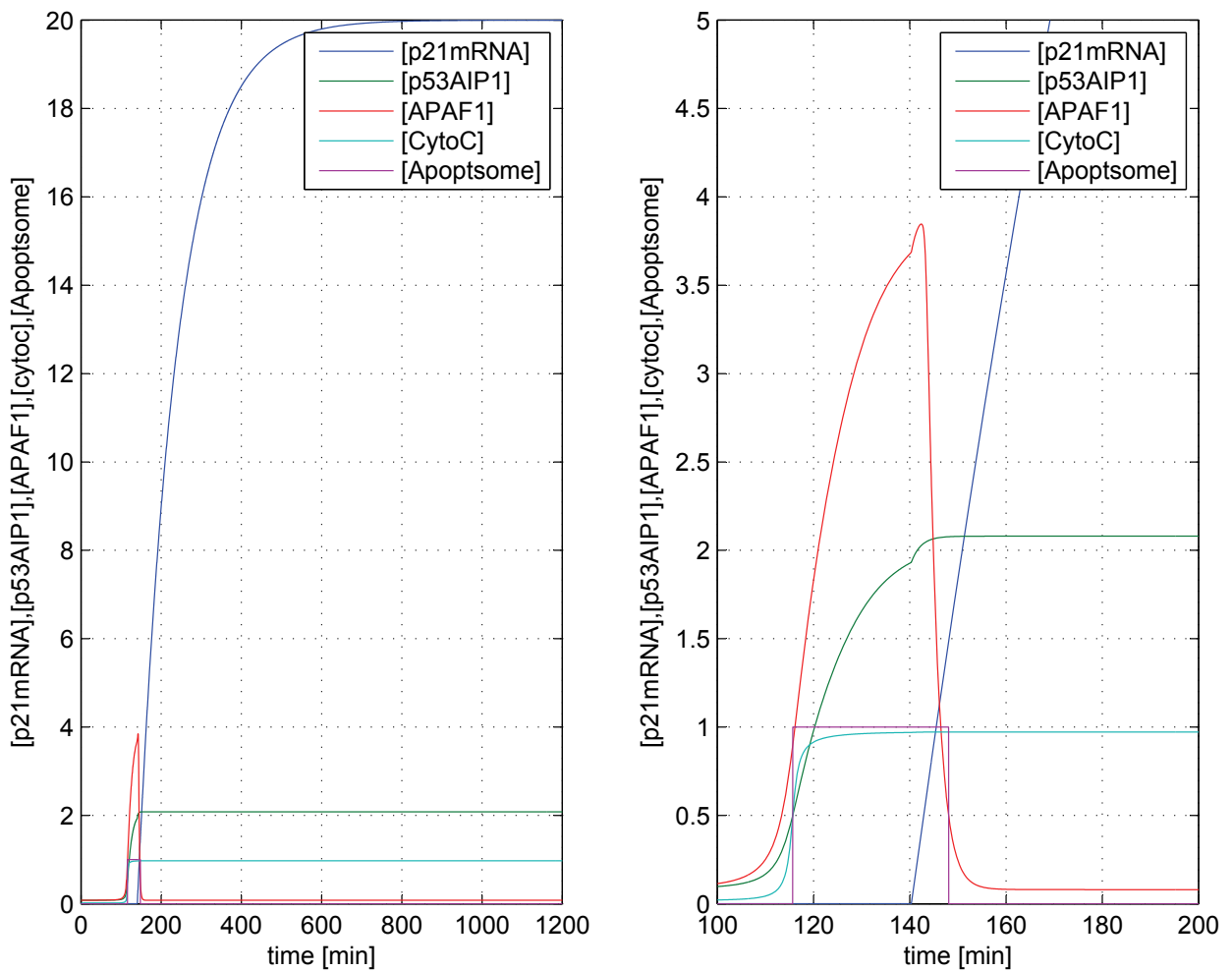


Figure 5: **Output response of apoptotic target genes network as a consequence of reversible DNA damage** - Left) all at once gene dynamics over the considered time-span of 1200min. p21mRNA overexpression is p53-independent and it triggers just in correspondence with the lowest time-rate values of the other species. Right) close-up view inside (partial) apoptotic time-window.

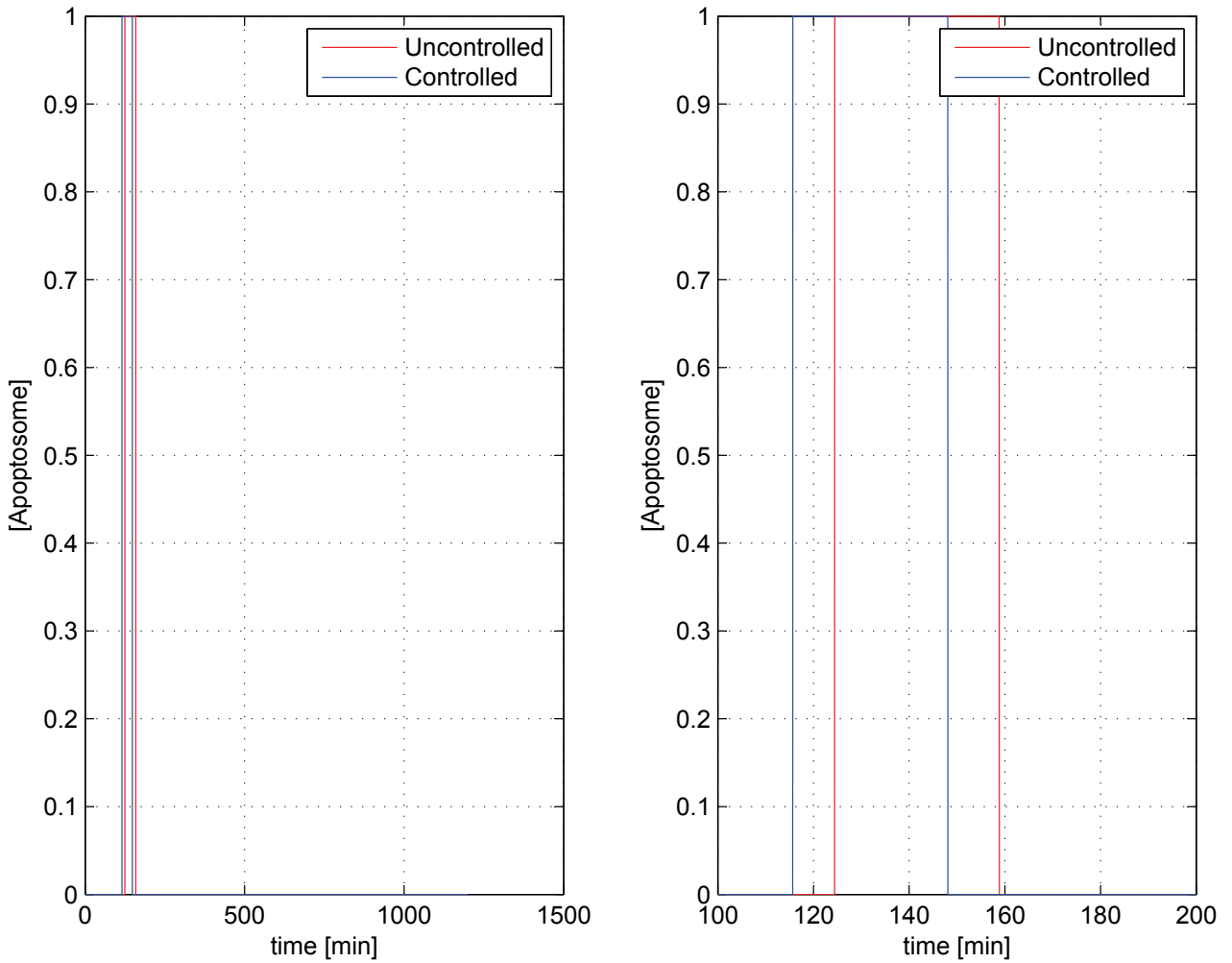


Figure 6: **Apoptosome digital response (reversible DNA damage)** - Left) Apoptotic instability occurs over the time-span  $114.4 \div 158.85$ min. This time-span is also divided into two sub-ranges. Right) The cell digital master simulator processes the normal (red) and highest (blue) DNA repairing action speeds. For the first case, the apoptotic time-window is  $114.4 \div 148$ min (uncontrolled); meanwhile, for the second one, the time-window is  $124.4 \div 158.85$  (controlled).

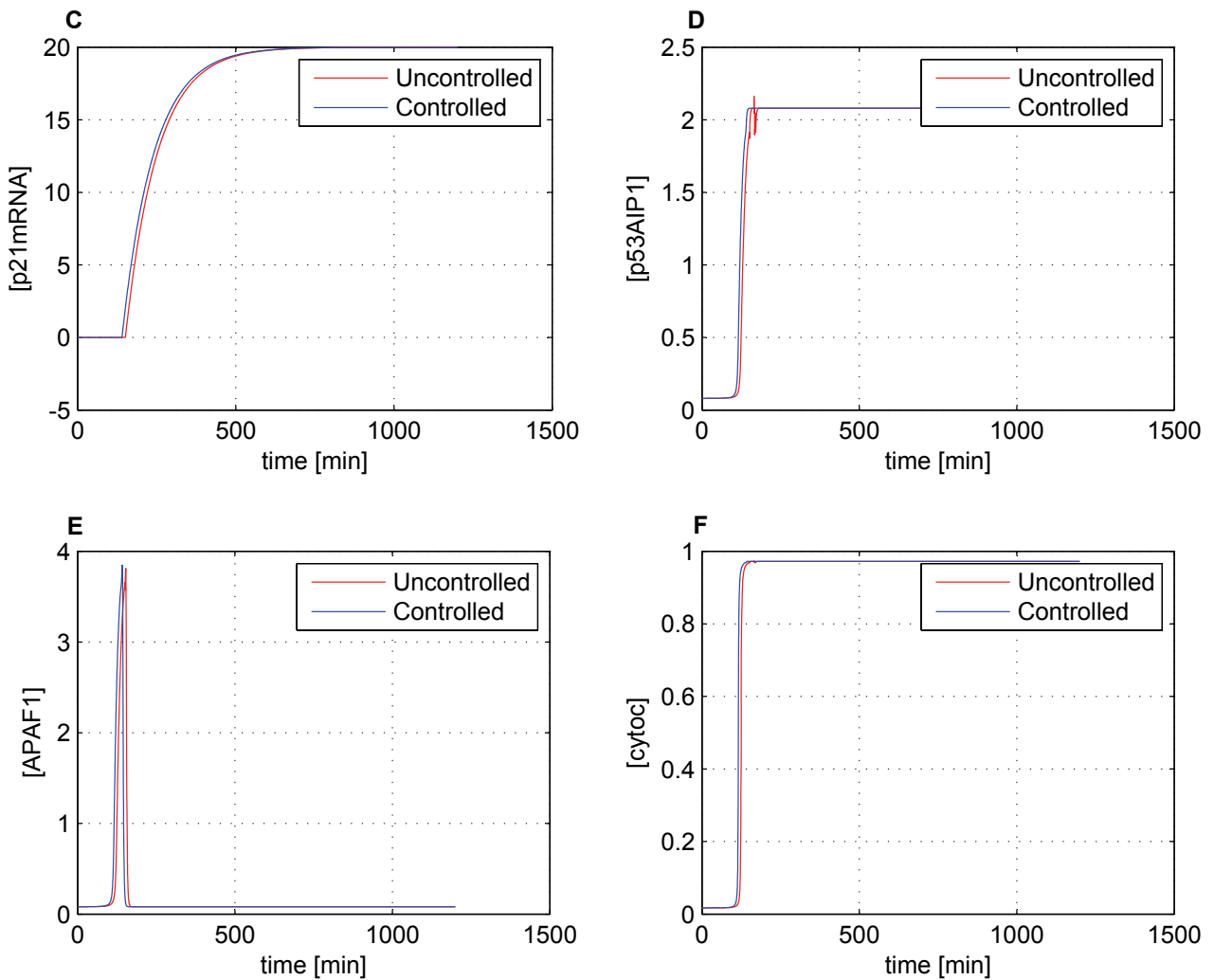


Figure 7: **Stand-alone apoptotic target gene dynamics (reversible DNA damage)** - c) p21mRNA overexpression both for the normal (red) and highest (blue) DNA repairing action speeds. Cell digital machinery confirms the p53-independence of p21mRNA and its "natural" upregulation after a DNA damage. d-f) p53AIP1, APAF1 and cytoc show very slight instabilities around apoptotic time-window (red). Cell digital machinery simulator (obviously) deletes instabilities (blue) but does not alter the gene pathways.

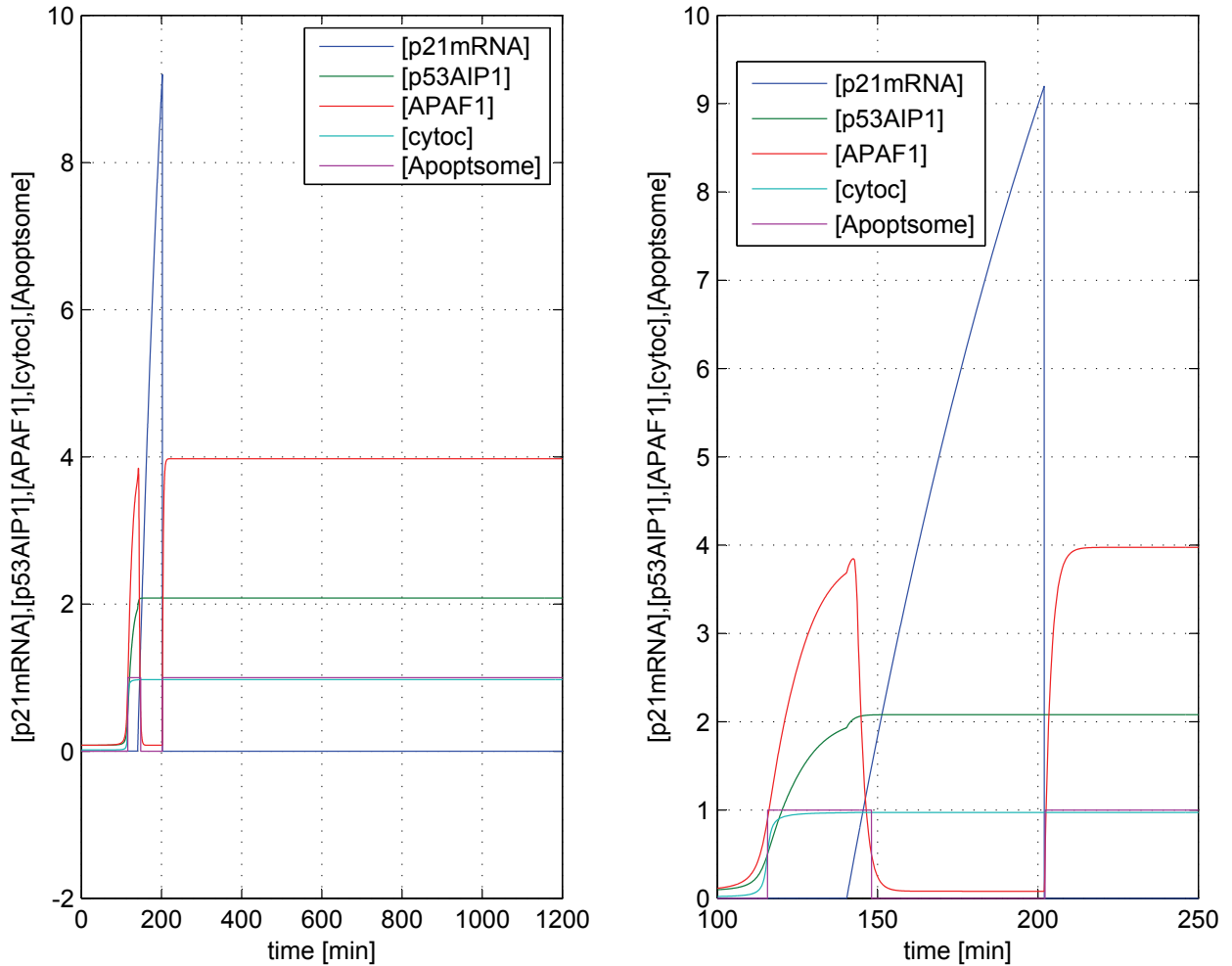


Figure 8: **Output response of apoptotic target genes network having as input a p21mRNA mono-cycle square-wave signal over a time-span of 0÷200min** - Left) all at once gene dynamics over the considered time-span of 1200min. p21mRNA overexpression oscillates to track the inflexion points of APAF1 double pulses. Right) Apoptosis is in phase-delay with p21mRNA starting overexpression. Apoptosome shows two distinct pulses.

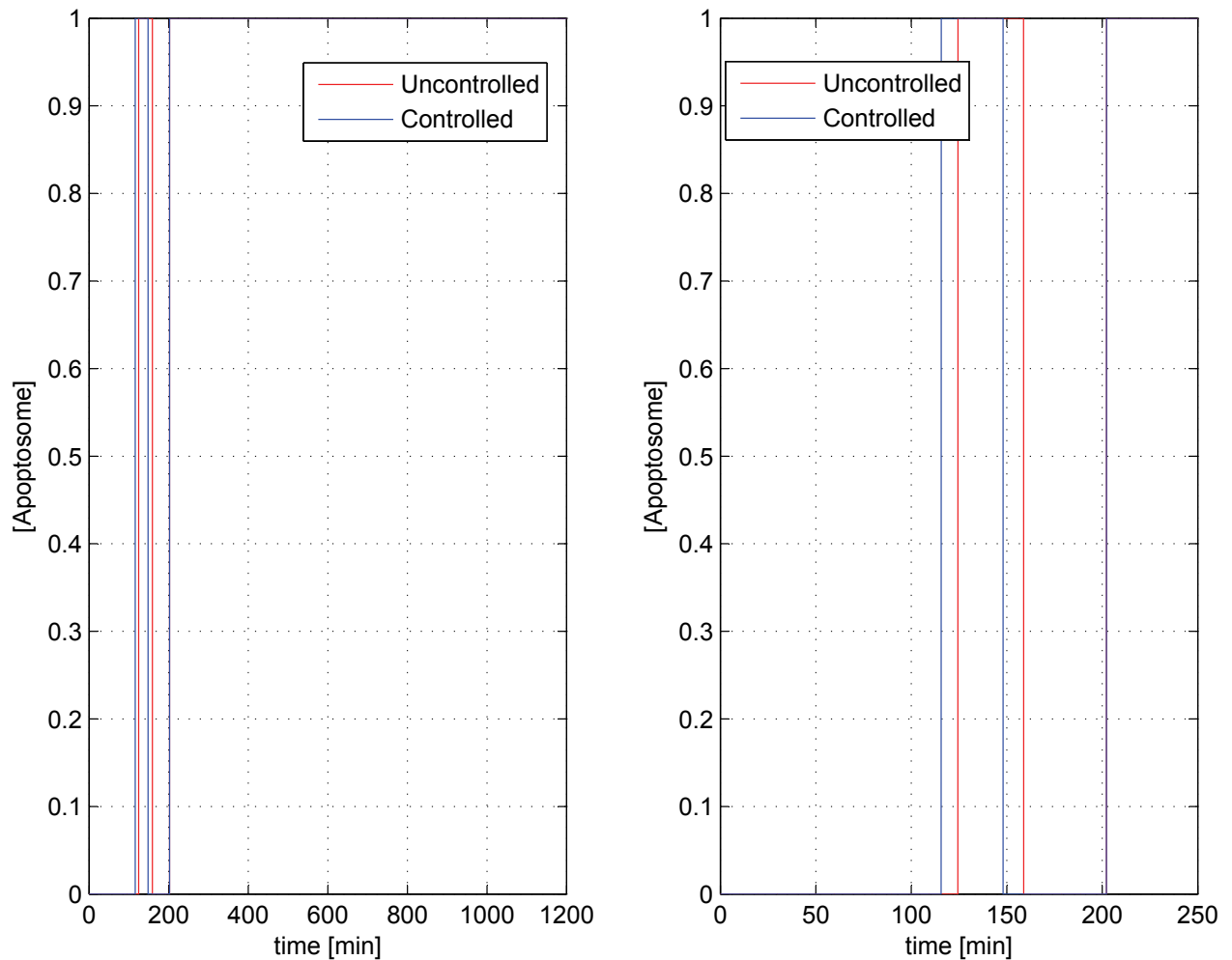


Figure 9: **Apoptosome digital response (irreversible DNA damage)** - Left) Apoptosis shows two pulses and reaches steady-stable condition. This phase is independent of DNA damage repair speed and it starts at 202.2min (merging red and blue) after the impulse of ionizing radiation. The apoptotic steady-state is not affected by the digital process involved in the cell master simulator. Right) Both pulses of Apoptosome lead to a stable-steady condition for apoptosis. Natural (red) and optimal (blue) digital pulses show an inter-pulse delay of 8.75min.

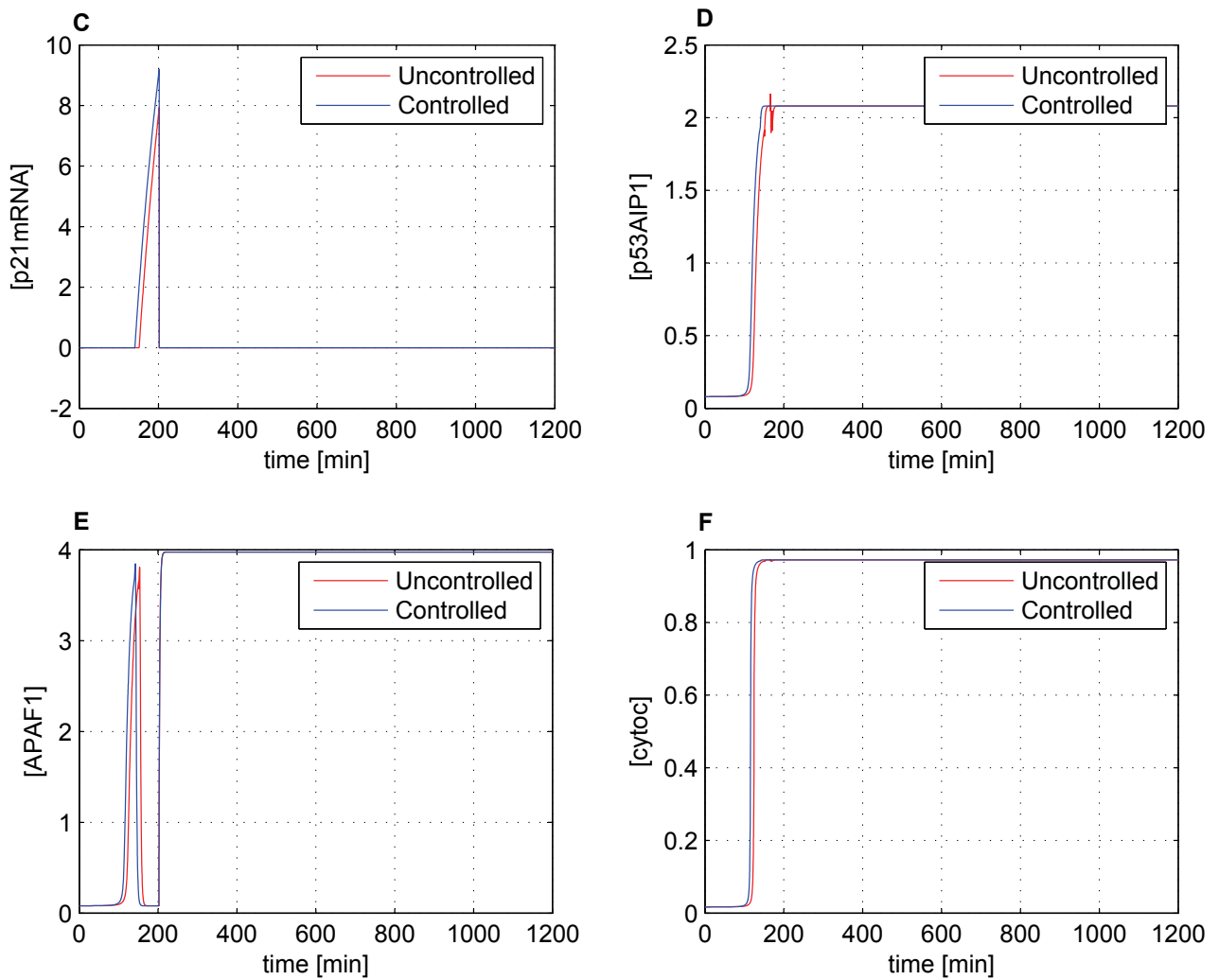


Figure 10: **Stand-alone apoptotic target gene dynamics - p21mRNA mono-cycle square-wave signal over a time-span of 0 ÷ 200min** - c) p21mRNA overexpression both for the normal (red) and highest (blue) DNA repairing action speeds. Cell digital machinery detects natural p21mRNA overexpression is lower (red) than the optimal time rate (blue) after a DNA damage. d-f) p53AIP1, APAF1 and cytoc show very slight instabilities around apoptotic time-window (red). Cell digital machinery simulator reproduces two pulses of APAF1. Both the natural (red) and optimal (blue) second pulse of APAF1 are merging at the end of p21mRNA mono-cycle signal input (200min).

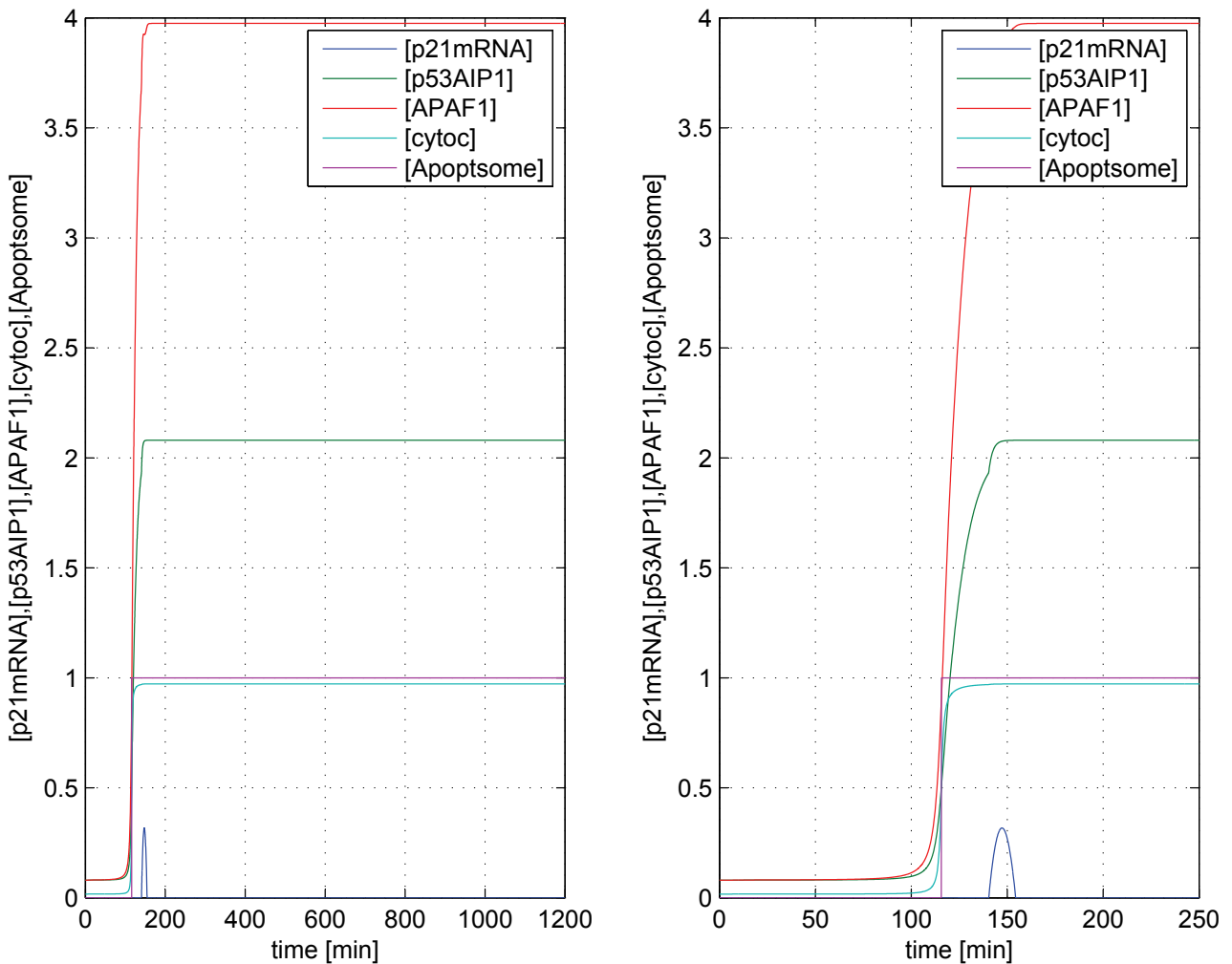


Figure 11: **Output response of apoptotic target gene network having as input a p21mRNA negative linear-ramp signal in-phase with apoptotic natural time-span of  $114.4 \div 144.85$ min** - Left) all at once gene dynamics shows relative saturation levels and has a choral inflexion point; then, apoptosis phase starts. p21mRNA overexpression is almost vanishing. Right) p21mRNA overexpression tracking properties are lost. Apoptosis triggers in-phase with choral inflexion points.

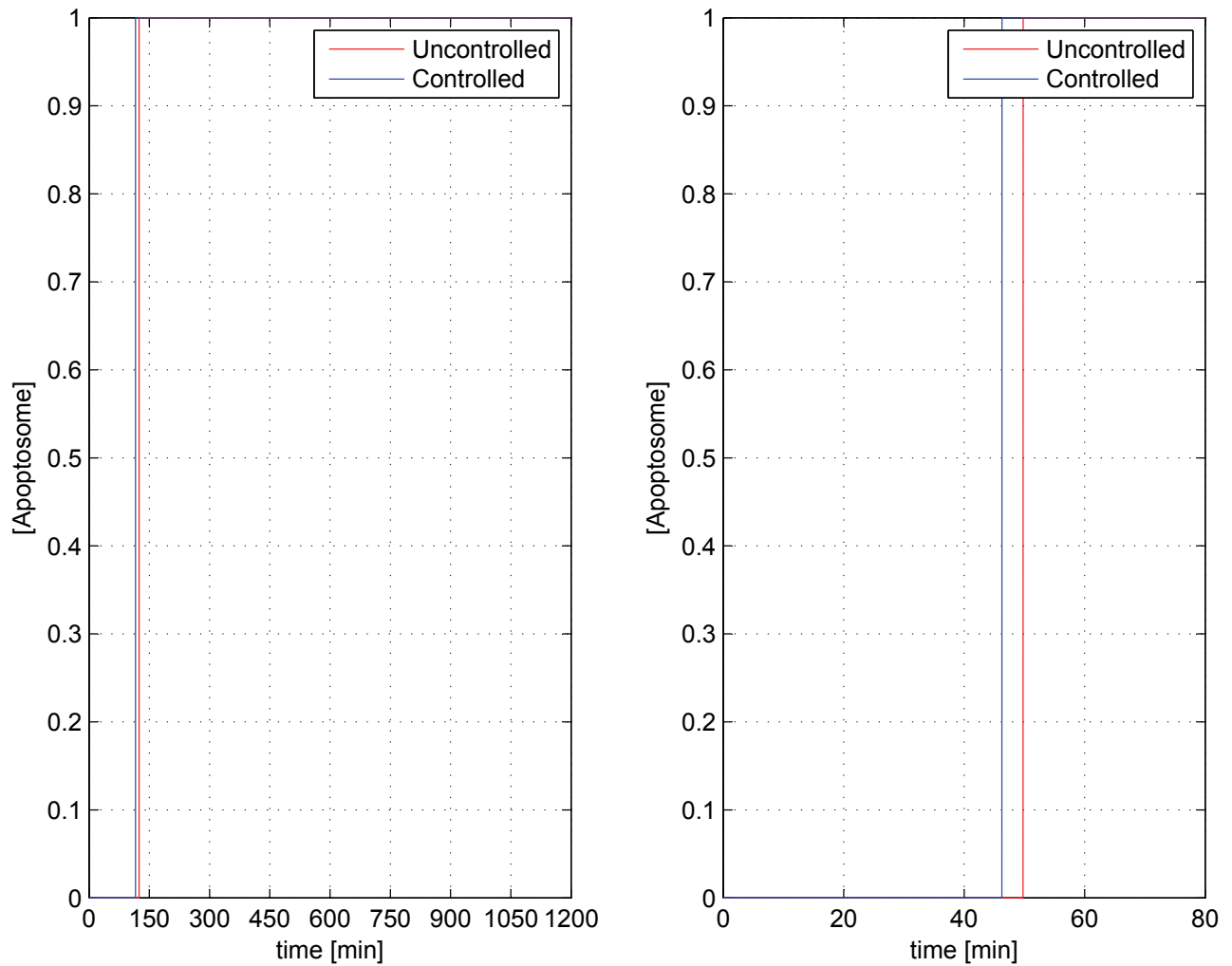


Figure 12: **Apoptosome digital response (irreversible DNA damage)** - Left) Both natural (red) and optimal (blue) DNA damage repair speeds allow mono-cycle stable-state apoptosis phase. Right) Natural DNA repair speed (red) admits apoptosis steady-state phase beginning at 124.4min; while, the optimal one allows the apoptosis starting from 115.65min.

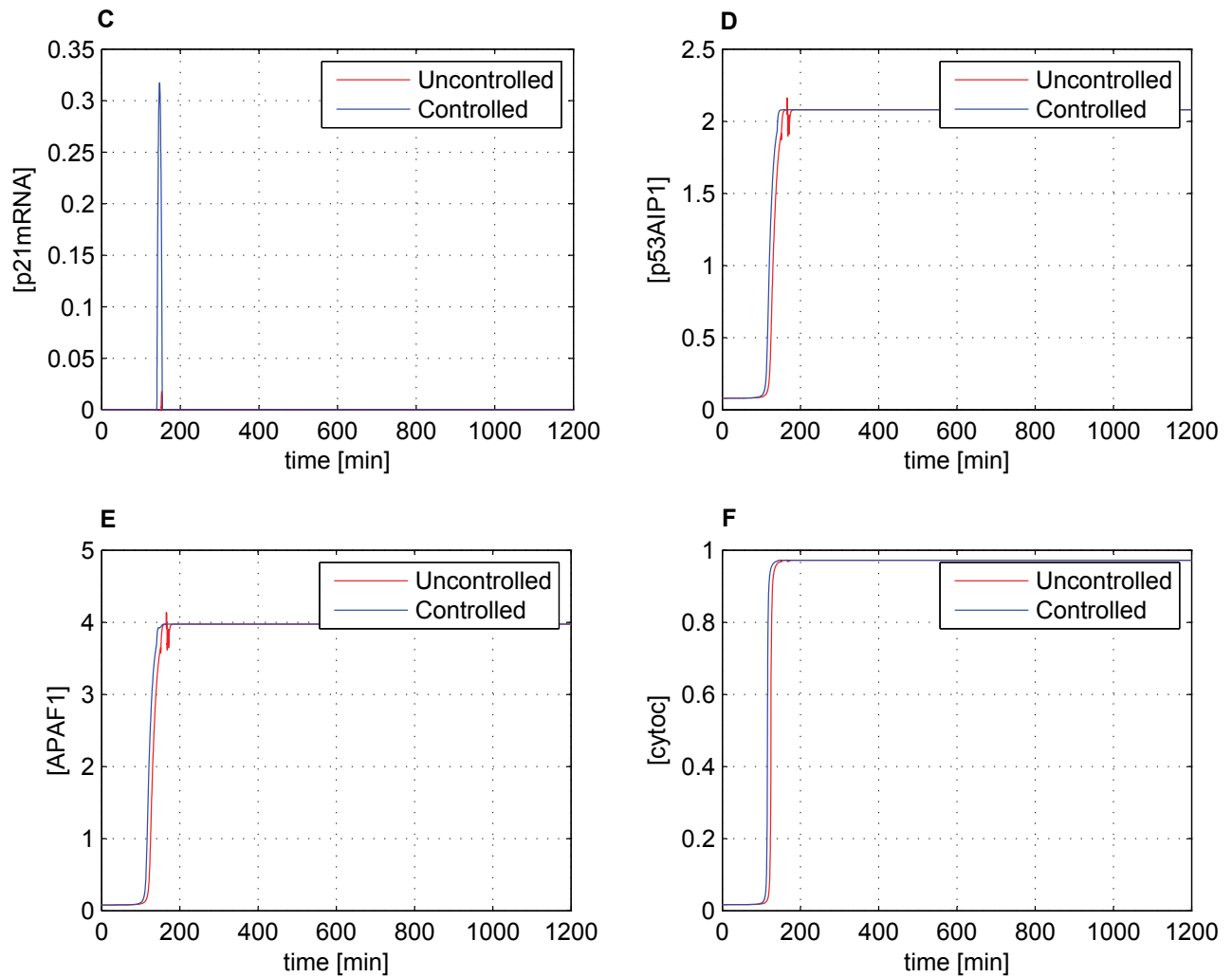


Figure 13: **Stand-alone apoptotic target genes dynamics - p21mRNA negative linear-ramp signal in-phase with apoptotic natural time-span of  $114.4 \div 144.85$ min** - c-f) Cell digital master simulator does not affect the response of the apoptotic target genes network. Only numerical instabilities are damped by the cell digital processor.

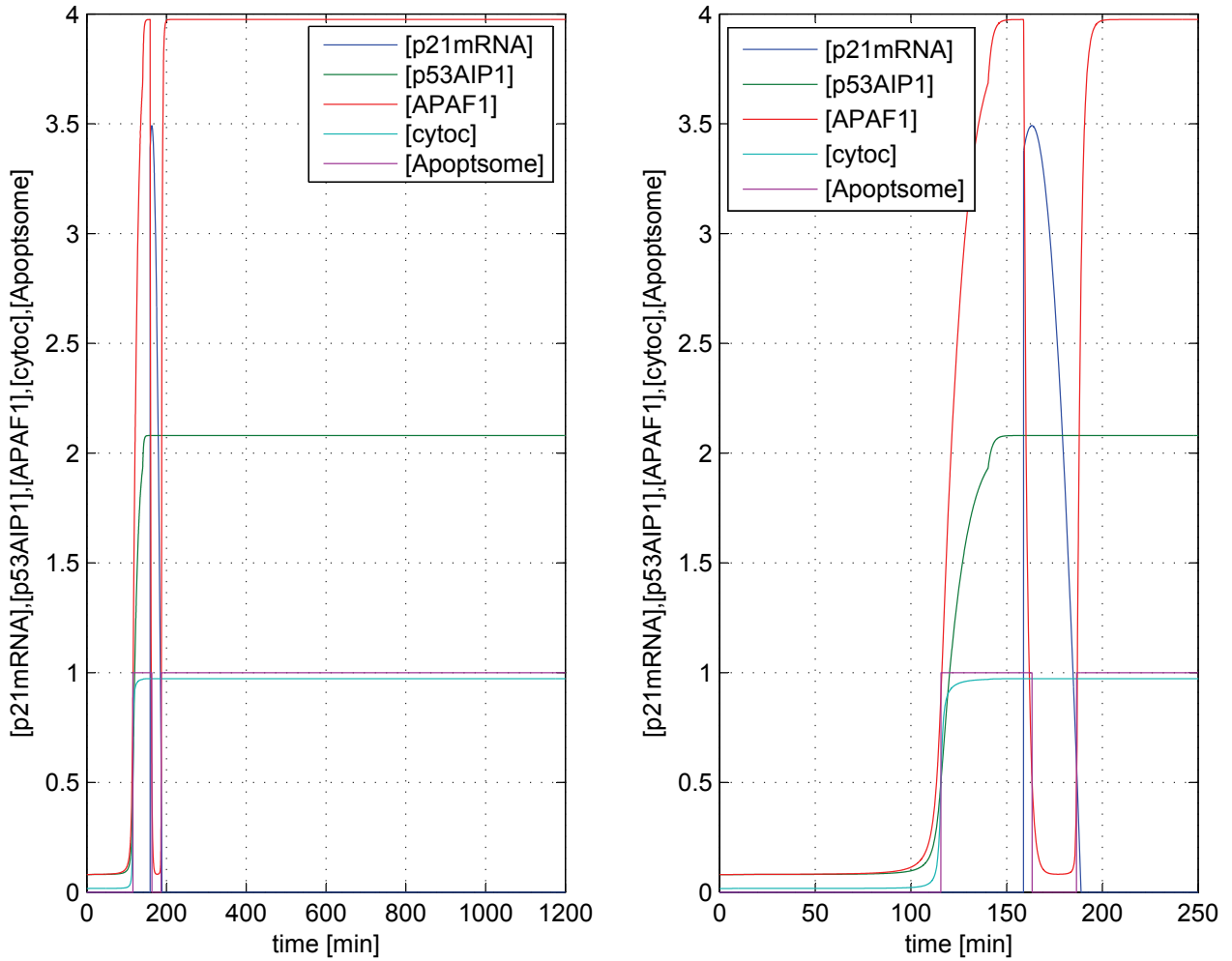


Figure 14: **Output response of apoptotic target gene network having as input a p21mRNA negative linear-ramp signal applied at the end of apoptotic natural time-span of 114.4÷144.85min** - From left to right) results are almost the same of the case shown in Figures 11-13 (p21mRNA mono cycle-wave signal over a time-span of 0÷200min).

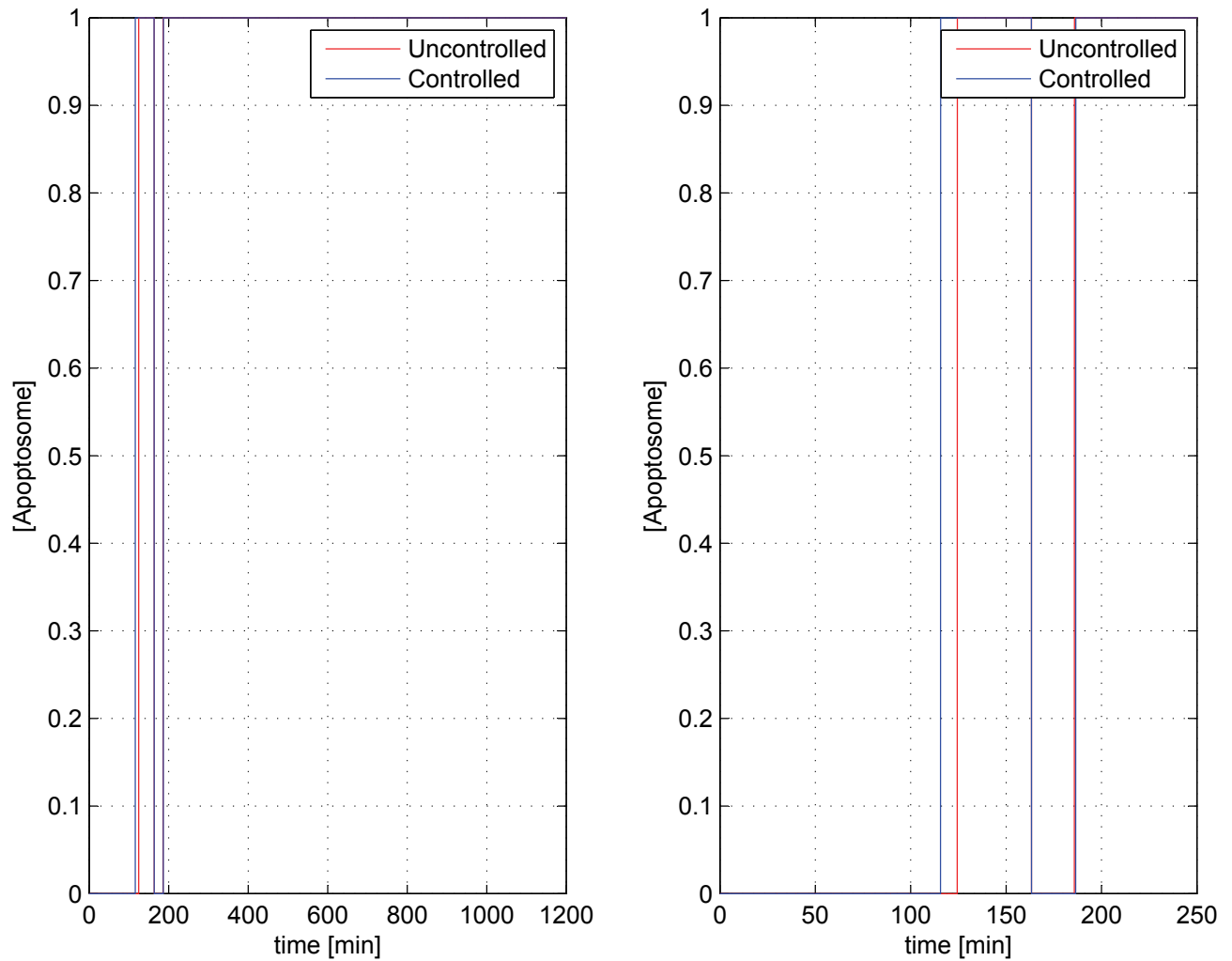


Figure 15: Apoptosome digital response - p21mRNA negative linear-ramp signal applied at the end of apoptotic natural time-span of  $114.4 \div 144.85$ min - The apoptotic time-windows remain exactly the same as in the case of Figures 11-13.

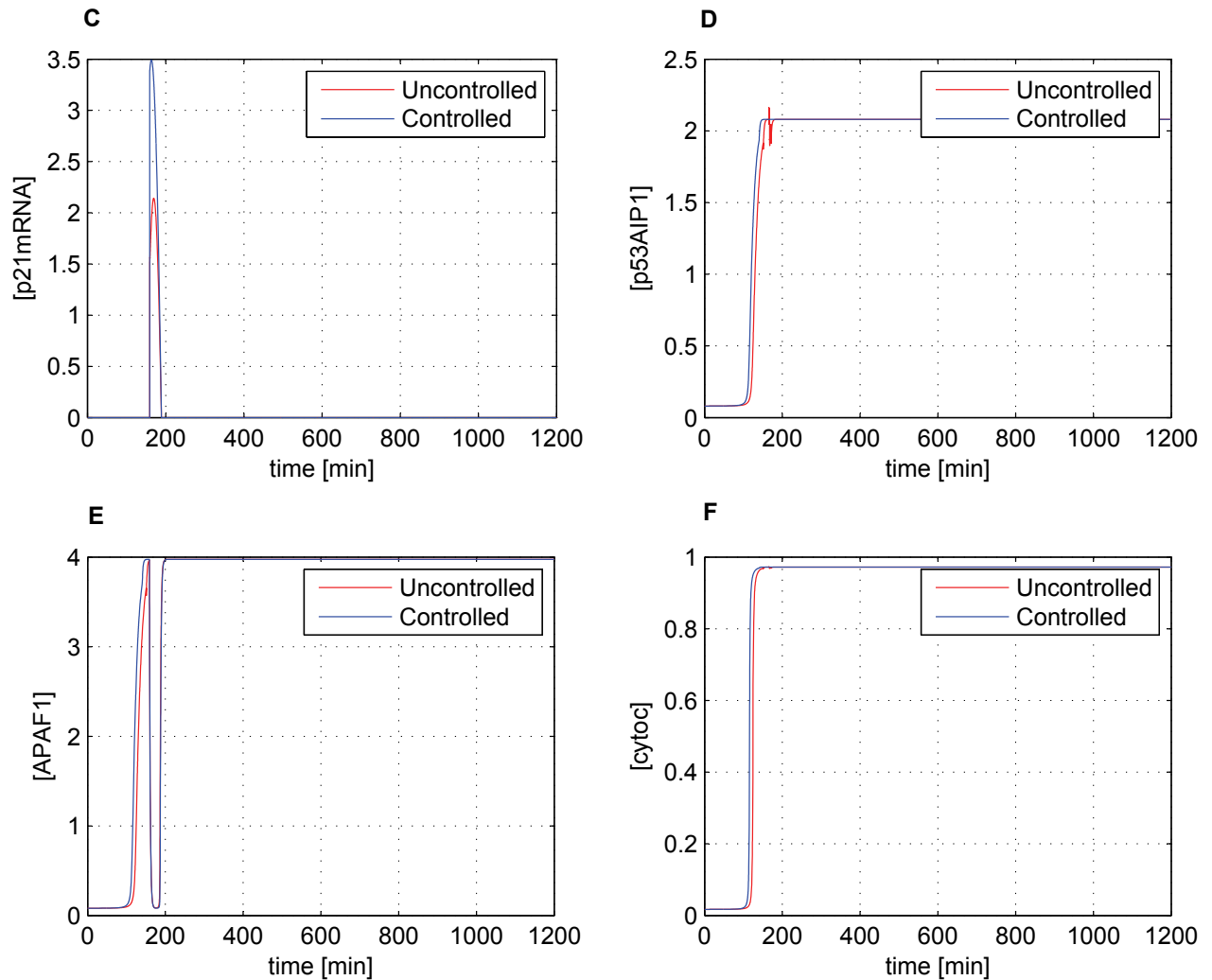


Figure 16: **Stand-alone apoptotic target genes dynamics - p21mRNA negative linear-ramp signal applied at the end of apoptotic natural time-span of 114.4 ÷ 144.85min** - c) to f) Results are almost the same as Figures 11-13 when output response of apoptotic target gene network having as input a p21mRNA mono-cycle square-wave signal over a time-span of 0 ÷ 200min has been investigated. p21mRNA runs like an interceptor and its tracking properties are again confirmed. The apoptotic time-windows remain exactly the same as in the case of Figures 11-13 when a mono-cycle square-wave signal has been employed to feature the p21mRNA pathway. The only difference consists of the overexpression of APAF1 within its two pulses.

tion could lead to a study for clarifying the importance of p21WAF1/CIP1(p21) gene expression in the tumorigenicity of hepatitis B virus (HBV) and hepatitis C virus (HCV) infected human hepatocellular carcinoma (HCC) or help to address new areas of research on the controversial aspect of the pathogenesis of Duchenne muscular dystrophy (DMD) in which abnormalities in proliferation and differentiation of the dystrophin-deficient muscle are observed. Analyses of molecules involved in cell cycle modulation do not actually exist in this context or are quite rare. In this pathology, cells withdrawn from the cell cycle permanently express p21. As recognized, p21, in contrast to other cell cycle proteins, does not diminish when myotubes are re-exposed to growth media and it has been statistically recognized that increased p21mRNA levels occur in dystrophin-deficient muscle tissue.

In conclusion, this paper attaches meaning to one way of thinking in science, the *inductive*. Even though great weight is given to biological experiments in this work to check its reliability, our engineering frame of mind and available resources (which lie in aerospace technologies) make necessary and almost compulsory the decision to use digital approaches to elucidate biology.

**Acknowledgement:** Marzia Sabella at the Department of Justice of Palermo (Italy) and Notre Dame du Cap de La Madeleine made this work possible.

## Reference

- [1]Ma L, Wagner J, Rice J-J, Hu W, Levine A-J, Stlovitzky G (2005) A plausible model for the digital response of p53 to DNA damage. *Proc Natl Acad Sci USA* 40:14266-14271.
- [2]Geva-Zatorsky N, Rosenfeld N, Itzkovitz S, Milo R, Sigal A, Dekel E, Yarnitzky T, Liron Y, Polak P, Lahav G, Alon U (2006) Oscillations and variability in the p53 system. *Molec Syst Biol*:doi: 10.1038
- [3]Shangary S, Wang S (2008) Targeting the Mdm2-p53 interaction for cancer therapy. *Clin Cancer Research* 17:5318-5324.
- [4]Ciliberto A, Novak B, Tyson J-J (2005) Steady states and oscillations in the p53/Mdm2 network. *Cell Cycle* 3:488-493.
- [5]Zhang T, Brazhnik P, Tyson J-J (2007) Exploring mechanisms of the DNA-damage response. *Cell Cycle* 1:85-94.
- [6]Knudson A-G (1971) Mutation and cancer: statistical study of retinoblastoma. *Proc Natl Acad Sci USA* 68:820-823.
- [7]Fodde R, Smits R (2002) A matter of dosage. *Science* 298:761-763.
- [8]Hohenstein P (2004) Tumour suppressor genes-one hit can be enough. *PLoS Biol* 2:165-166.
- [9]Venkatachalan S, Shi Y-P, Jones S-N, Vogel H, Bradley A, Pinkel D (1998) Retention of wild-type p53 in tumours from p53 heterozygous mice: reduction of p53 dosage can promote cancer formation. *EMBO J* 17:4657-4667.
- [10]Song W-J (1999) Haploinsufficiency CBFA2 causes familial thrombocytopenia with propensity to develop acute myelogenous leukaemia. *Nature Genet* 23:166-175.
- [11]Reich C-N, Oren M, Levine A-J (1983) Two distinct mechanisms regulate the levels of a cellular tumor antigen, p53. *Mol Cell Biol* 12:2143-2150.
- [12]Bates S, Phillips A-C, Clark P-A, Stott F, Peters G, Ludwig R-L, Vousden K-H (1998) p14ARF links the tumour suppressor RB and p53. *Nature* 395:124-125.
- [13]Bar-Or R-L, Maya R, Segel L-A, Alon U, Levine A-J, Oren M (2000) Generation of oscillations by the p53-Mdm2 feedback loop: a theoretical and experimental study. *Proc Natl Acad Sci USA* 21:11250-11255.
- [14]Bell S, Klein C, Muller L, Hansen S, Buchner J (2002) p53 contains large unstructured regions in its native state. *J Mol Biol* 322:917-927.
- [15]Lahav G, Rosenfeld N, Sigal A, Geva-Zatorsky N, Levine A-J, Elowitz M-B,

- Alon U (2004) Dynamics of the p53-Mdm2 feedback loop in individual cells. *Nature Genetics*:doi 10.1038 - published online (www.nature.com/naturegenetics)
- [16]Loewer A, Lahav G (2006) Cellular conference call: external feedback affect cell-fate decision. *Cell* 24:1128-1130.
- [17]Ventura A, Kirsch D-G, McLaughlin M-E, Tuveson D-A, Grimm J, Lintault L, Newman J, Reczek E-E, Weissleder R, Jacks T (2007) Restoration of p53 function leads to tumour regression in vivo. *Nature* 445:661-665.
- [18]Batchelor E, Mock C-S, Bhan I, Loewer A, Lahav G (2008) Recurrent initiation: a mechanism for triggering p53 pulses in response to DNA damage. *Mol Cell* 30:277-289.
- [19]Ghosh B, Bose I (2006) Gene copy number and cell cycle arrest. *Phys Biol* 3:29-36.
- [20]Bose I, Ghosh B (2007) The p53-MDM2 network: from oscillations to apoptosis. *J Biosci* 32:991-997.
- [21]Ardito Marretta R-M, Marino F (2007) Wing flutter suppression enhancement using a well-suited active control model. *J Aero Engng* 221:441-453.
- [22]Ardito Marretta R-M, Marino F, Bianchi P (2008) Computer active control of damping fluid of a racing superbike suspension scheme for road-safety improvement spin-off. *J Vehicle Design* 46:436-450.
- [23]Ardito Marretta R-M, Barbaraci G (2009) Digital control circuitry of cancer cell and its apoptosis. *Molecular and Cell Biomechanics* 6: (in press).
- [24]Vassilev L-T, Vu B-T, Graves B, Carvajal D, Podlaski F, Filipovic Z, Kong N, Kammlott U, Lukacs C, Klein C, Fotouhi N, Liu EA (2004) In vivo activation of the p53 pathway by small-molecule antagonist of Mdm2. *Science* 303:1889-1893.
- [25]Meek D-W (2002) The p53 response to DNA damage. *DNA Repair (Amst)* 3:1049-1056 (2004).
- [26]Vousden K-H, Lu X (2002) Live or let die. The cell's response to p53. *Nat Rev Cancer* 2:594-604.
- [27]Haupr S, Berger M, Goldberg Z, Haupr Y (2003) Apoptosis - the p53 network. *J Cell Sci* 116:4077-4085.
- [28]Fiscella M, Zhang H, Fan S, Sakaguchi K, Shen S, Mercer W-E, Vande Woude G-F, O'Connor P-M, Appella E (1997) Wip 1, a novel human protein phosphatase that is induced in response to ionizing radiation in a p53-dependent manner. *Proc Natl Acad Sci USA* 94:6043-6053.
- [29]Oda K, Atakawa H, Tanada T, Matsuda K, Tanikawa C, Mori T, Nishimori H, Tanai K, Tokino T, Nakamura Y, Taya Y (2000) p53AIP1, a potential mediator of p53-dependent apoptosis, and its regulation by SER-46 phosphorylated p53. *Cell* 102:849-862.
- [30]Viale A, De Franco F, Orleth A, Cambiaghi V, Giuliani V, Bossi D, Ronchini C, Ronzoni S, Muratore I, Monestiroli S, Gobbi A, Alcalay M, Minacci S, Pelicci P-G (2009) Cell-cycle restriction limits DNA damage and maintains self-renewal of leukaemia stem cells. *Nature* 457:51-57.
- [31]Tsourkas A, Weissleder R (2004) Illuminating the dynamics of intracellular activity with "active" molecular reporters. *Molecular and Cell Biomechanics* 1:136-146.
- [32]Deguchi S, Ohashi T, Sato M (2005) Intracellular stress transmission through actin stress fiber network in adherent vascular cells. *Molecular and Cell Biomechanics* 2:205-216.
- [33]Mooney D (2006) Materials to regulate cell fate in vitro and in vivo. *Molecular and Cell Biomechanics* 3:169-176.
- [34]Zhou J, Chen J-K, Zhang Y (2007) Theoretical analysis of thermal damage in biological tissues caused by laser irradiation. *Molecular and Cell Biomechanics* 4:27-40.

